การมีอยู่ของผลเฉลยของการไหลเนื่องจากการกระจายความดัน

นายรตินันท์ บุญเคลือบ
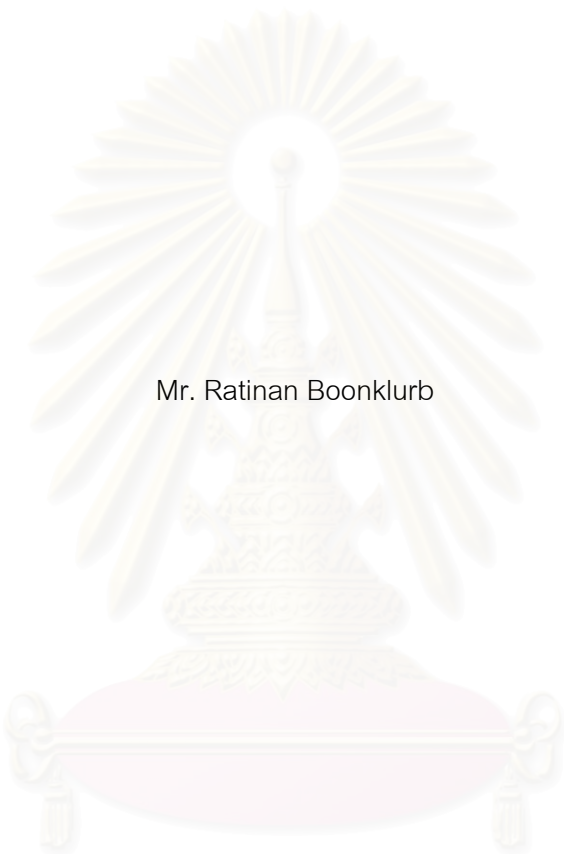
ON THE EXISTENCE OF SOLUTIONS OF FLOWS DUE TO PRESSURE DISTRIBUTION

Mr. Ratinan Boonklurb

Thesis Title   ON THE EXISTENCE OF SOLUTIONS OF FLOWS DUE TO

                            PRESSURE DISTRIBUTION

By   Mr. Ratinan Boonklurb

Field of study   Mathematics

Thesis Advisor   Assistant Professor Jack Asavanant, Ph.D.

Accepted by the Faculty of Science, Chulalongkorn University in Partial

Fulfillment of the Requirements for the Master 's Degree

………………………………………….. Deputy Dean for Administrative Affairs

(Associate Professor Pipat Karntiang, Ph.D.) Acting Dean, Faculty of Science

THESIS COMMITTEE

…………………………………………….. Chairman

(Assistant Professor Pornchai Satravaha, Ph.D.)

……………………………………….……. Thesis Advisor

(Assistant Professor Jack Asavanant, Ph.D.)

…………………………………………….. Member

(Dr. Vimolrat Ngamaramvaranggul, Ph.D.)

รตินันท์ บุญเคลือบ : การมีอยู่ของผลเฉลยของการไหลเนื่องจากการกระจายความดัน(ON THE EXISTENCE OF SOLUTIONS OF FLOWS DUE TO PRESSURE DISTRIBUTION) อ. ที่ปรึกษา : ผู้ช่วยศาสตราจารย์ ดร.จักษ์ อัศวานันท์, 52 หน้า. ISBN 974-03-1379-5.

เราพิจารณาการไหลในสองมิติ ที่เป็นอิสระจากเวลาภายใต้การกระจายความดันในน้ำที่มีความลึกจำกัด แรงโน้มถ่วงของโลกได้ถูกกำหนดในเงื่อนไขขอบเขต เราใช้ perturbation technique ทำให้ได้สมการ KdV ที่มีแรงมาเกี่ยวข้อง เราได้ตั้งและพิสูจน์ทฤษฎีบทที่เกี่ยวกับการมีอยู่ของผลเฉลยสำหรับสมการนี้ทุกกรณี นอกจากนั้นเราได้แก้ปัญหานี้โดยวิธีเชิงตัวเลขเพื่อเป็นการยืนยันทฤษฎีบทที่ได้พิสูจน์ไปข้างต้น โดยพบว่าในกรณีที่ Froude number มากกว่าหนึ่ง จะมีคำตอบสองคำตอบที่สอดคล้องกับค่า Froude number ค่าเดียวกัน เมื่อความดันมีค่าเป็นบวก และคำตอบมีเพียงคำตอบเดียวเมื่อความดันมีค่าเป็นลบ สำหรับกรณีที่ Froude number มีค่าน้อยกว่าหนึ่ง คำตอบจะมีคลื่นเกิดที่ด้านหลังของการกระจายความดัน ในกรณีนี้คลื่นจะหายไปเมื่อ Froude number มีค่าเข้าใกล้ค่าวิกฤตบางค่า

ภาควิชา **คณิตศาสตร์**	ลายมือชื่อนิสิต..
สาขาวิชา **คณิตศาสตร์**	ลายมือชื่ออาจารย์ที่ปรึกษา......................................
ปีการศึกษา 2544	ลายมือชื่ออาจารย์ที่ปรึกษาร่วม -

RATINAN BOONKLURB : ON THE EXISTENCE OF SOLUTIONS OF FLOWS DUE TO PRESSURE DISTRIBUTION. THESIS ADVISOR:ASSIST.PROF. JACK ASAVANANT, Ph.D., 52 pp. ISBN 974-03-1379-5.

Steady two-dimensional flows due to an applied pressure distribution in water of finite depth are considered. Gravity is included in the dynamic boundary condition. We use perturbation technique to derive the forced KdV equation. Existence theorems for different types of solution to this equation are given and proved. Numerical solutions are provided as the confirmation to these findings. There exist up to two solutions that correspond to the same value of Froude number greater than unity for positive pressure distributions, and a unique solution for negative pressure distribution. When the Froude number is less than unity, solutions are characterized by a train of waves behind the pressure distribution. These waves diminish when the Froude number approaches some critical values.

Department **Mathematics**	Student's signature..
Field of study **Mathematics**	Advisor's signature...
Academic year **2001**	Co-advisor's signature -

ACKNOWLEDGEMENTS

CONTENTS

CHAPTER I

Formulation of Flows with Gravity

1.1   Introduction

Efforts to analyze the hydrodynamical characteristic of free-surface flow with surface disturbance have been divided primarily between theoretical and experimental considerations. There are various types of surface-disturbance occurred in nature whereas some are often due to man-made structures. Most of the theoretical studies lie mainly in the two-dimensional framework and are based on global analysis. Results from the laboratory experiments provide, on the other hand, small scale analysis for both two- and three-dimensional problems.

We devote this research to the investigation of steady two-dimensional potential flow of an inviscid and incompressible fluid due to pressure distribution. This two-dimensional model allows us to utilize various mathematical tools for solving the problem. For example, the asymptotic analysis particularly perturbation technique has been successfully employed to solve linear and nonlinear water wave problems. This simplification will provide not only qualitative behaviors but also some insights to the real flow situations. Though the assumption of steadiness may seem unreal but we can always choose the appropriate moving frame of reference in such a way that the flow becomes steady.

Here, we seek the weakly nonlinear solutions of free-surface flow past an applied pressure distribution on the free-surface. The fluid domain is of finite depth with no vertical boundaries in the far fields. Such flows can be produced by

blowing air on the surface of water flowing in the channel with parallel side walls. Far upstream, the flow is assumed to approach a uniform stream with constant velocity U and uniform depth H. The flow is characterized by a nondimensional parameter, the Froude number,

$$F = \frac{U}{\sqrt{gH}}.$$

In general, this flow configuration can be served as a model of moving vehicles such as hovercraft in a long canal. It may also be viewed as an inverse method of solution to the classical ship-wave problem. When the pressure distribution is applied, the free surface will deform in the neighborhood (probably with downstream influence) of the applied pressure distribution. This resembles the problem of flow past a rigid obstacle.

The problem of free surface pressure distributions has been studied quite extensively in the case of infinite depth for over 150 years. The classical linearized version of the two dimensional problem was solved long ago and was discussed in detail by Lamb (1932). It was shown that for some pressure distributions the motion is drag-free. That is, the free surface is symmetric with respect to the applied pressure distribution without a train of sinusoidal waves in the far field. Schwartz (1981) reformulated the problem into a boundary integral equation technique based on Cauchy's integral formula and solved numerically. Fluid was assumed to be of infinite depth. He showed that nonlinear theory gave drag-free solution at certain values of the span length of pressure distribution ($L = \dfrac{2}{F^2} = 4\pi, 8\pi, ...$), i.e. when the ship length was an integer multiple of a free wave length while linearized theory did not. He also found nonlinear wave train in the form of narrow crests and broad troughs which were essentially periodic and propagated downstream.

In the case of finite depth, Von-Kerczek and Salvesen (1977) placed a network

of mesh points over the entire flow domain and performed finite difference calculations (successive overrelaxation) to obtain nonlinear solutions. Their numerical calculations were restricted to certain values of the ratio of pressure-distribution-length to the depth of the flow domain. The nonlinear wave train propagates downstream while the flow satisfies radiation condition on the upstream free surface. Drag-free (symmetric) solutions were found at the critical Froude number F'_* ($0 < F'_* < 1$). It should be noted here that they defined the Froude number based on the span length of pressure distribution which is different from ours. Solutions at two critical values of Froude number, $0 < F'_{*2} < F'_{*1} < 1$, were presented for various values of magnitude of pressure distribution. When $F > F'_{*1}$, the wave resistance increased to their maximum value and then decreased as $F \to 1$. When $F'_{*2} < F < F'_{*1}$, the wave resistance increased to their peak and decreased as F approach F'_{*2}. In addition, they found a *hump* on the free surface as $F \to F'_{*1}$ while two *humps* were detected as $F \to F'_{*2}$. They also found that, the effect of the non-linearities can clearly be seen on the phase shift in the solutions. Asavanant, et, al.(2001) reconsidered the problem by only putting mesh points on the free surface and using the boundary integral technique to find fully nonlinear solutions. The condition of incompressibility and irrotationality of the fluid motion implied the existence of the potential function and stream function. The fluid domain in the physical plane was transformed onto the complex plane. Bernoulli equation was applied on the free surface while they assumed no flow across the bottom boundary. They satisfied the bottom condition by using Schwartz reflection principle. Their results showed that, for both supercritical and subcritical flows, solutions were characterized by three parameters : (i) Froude number (ii) magnitude of the applied pressure distribution and (iii) span length of the applied pressure distribution. For supercritical flows ($F > 1$), they found up to two solution corresponding

to the same value of F for positive pressures (one was a perturbation of uniform stream and the other solution was perturbation of the solitary wave solution). They also found a unique solution for negative pressures. For subcritical flows they found a train of nonlinear waves behind the applied pressure distribution. The wave resistance decreased as F decreased. The wave resistance ultimately became zero when the critical value F_{*1} of F was reached. For $F < F_{*1}$, the wave resistance increased to another local maximum value and then decreased monotonically to zero again at $F = F_{*2}$. In addition, the free surface, upon which the pressure distribution was applied, deformed into two *humps*. This cycle of behavior repeatedly occurred as F reached another critical value. They conjecture that there were finitely many critical Froude numbers $0 < ... < F_{*2} < F_{*1} < 1$ such that drag-free solution exist. Moreover, there were n *humps* on the free surface for solution with $F_{*n} < F < F_{*n-1}$.

Inverse problem to flows due to applied pressure distribution is the problem of flows over a semi-circular obstruction considered by Forbes and Schwartz (1982). They constructed an integral equation involving flows variables at the free surface so that the bottom boundary condition is automatically satisfied. The exact nonlinear equations were solved numerically by a process of Newtonian iterations. In the subcritical case, they showed that there exist flows with essentially no waves on the upstream side and the train of nonlinear Stokes waves on the downstream side. When the circle radius increased or $F \uparrow 1$, the wave amplitude increased. In the supercritical case, they found symmetric solutions with respect to the axis of symmetry of the semicircle. For a large value of F, the nonlinear free surface profile is ultimately limited by the formation of a sharp crest with sides enclosing an angle $120°$.

Asavanant and Vanden-Broeck (1994) studied the steady two-dimensional flow

past a parabolic obstacle lying on the free surface in water of finite depth. The object was described by $y = \frac{1}{2}\epsilon(x - x_0)^2 + y_0$. Here (x_0, y_0) represented the vertex of the object and ϵ was the object geometry (object was concave if $\epsilon > 0$, convex if $\epsilon < 0$ and flat if $\epsilon = 0$). The problem was solved numerically by using boundary integral equation technique based on the Cauchy's integral formula. An integral equation was solved together with the dynamic free-surface condition. The bottom boundary condition was satisfied by employing the reflection principle. For supercritical flow past the concave object ($F > 1$, $\epsilon > 0$), they found two different types of solutions. The first one is the vertex of the obstacle was below the level of the free surface at infinity. These solution modelled a ship moving at a constant velocity in the channel. These solutions exist for all value of F ($1 \leq F^2 < \infty$). The second one was the vertex of the obstacle was above the level of the free surface at infinity. This solution modelled a surfboard riding on the wave. For supercritical flows past a convex object ($F > 1$, $\epsilon < 0$), they found one type of solution. Their numerical results showed that there were nonuniqueness of solutions corresponding to the same value of F. They concluded that one solution was a perturbation of uniform stream while the other solution was a perturbation of solitary wave solution. Their subcritical solutions showed that a train of (linear) sine waves was generated for large value of F. These waves developed narrow crests and broad troughs as F decreased. Finally, they conjectured that these waves would approach their limiting configurations characterized by a 120° angle corner at the crest.

From above, we can realize that problems in free-surface hydrodynamics under the influence of gravity are too usually difficult to solve exactly. Appropriate techniques of mathematical approximations are generally sought. Here, we use asymptotic approximations in the primitive variables to derive the forced KdV

equation. Existence theorem for different types of solution to this equation will be given and proved. Finally, numerical solutions are provided as the confirmation to these findings.

1.2   Formulation

We consider the steady two-dimensional, irrotational flow of an inviscid incompressible fluid in the domain bounded below by a rigid bottom and above by a free surface as shown in Figure 1.1. We choose Cartesian coordinates with the X-axis along the free surface at $x = -\infty$ and the Y-axis directed vertically upwards through the symmetry line of the applied pressure distribution. Gravity is acting in the negative Y-direction. The velocity components in the X- and Y-direction are denoted by u and v respectively. As $x \to -\infty$, the flow is assumed to approach a uniform stream with constant velocity U^* and constant depth H. The governing equations and boundary conditions are given by the following Euler equations :

$$u^*_{x^*} + v^*_{y^*} = 0$$

$$u^* u^*_{x^*} + v^* u^*_{y^*} = \frac{-p^*_{x^*}}{\rho}$$

$$u^* v^*_{x^*} + v^* v^*_{y^*} = \frac{-p^*_{y^*}}{\rho} - g$$

at the bottom $y^* = -H$; $\qquad\qquad v^* = 0$

at the surface $y^* = \eta^*$; $\qquad u^* \eta^*_{x^*} - v^* = 0$

$$p^* = b^*(x^*) \text{ with compact support}$$

where u^* and v^* are horizontal and vertical velocities, p^* is pressure, g is the gravitational acceleration, ρ is the density of the fluid and all the subscripts denote derivative with respect to corresponding variable. We define the following non-dimensional variables:
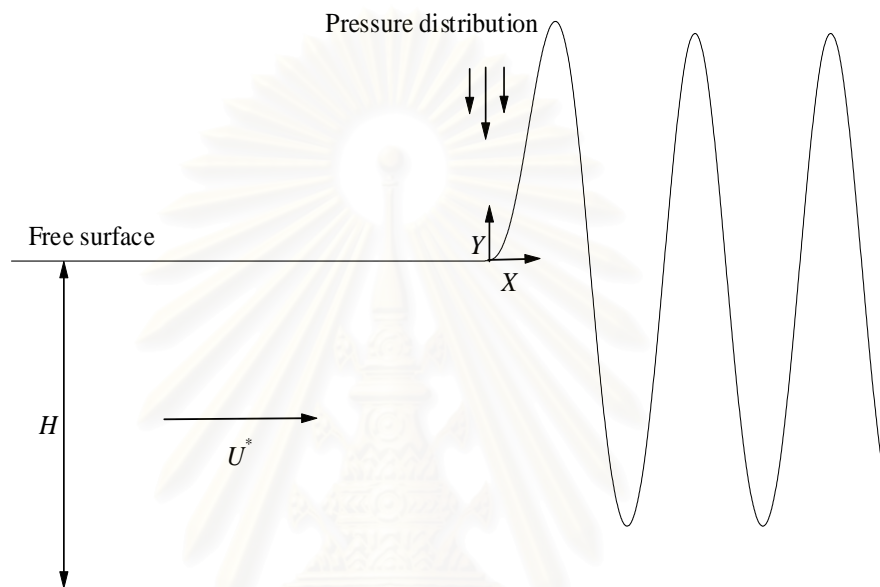
Figure 1.1: Sketch of flow domain under the applied pressure distribution.

$$\eta = \frac{\varepsilon^{-1}\eta^*}{H} \ , \ \ p = \frac{p^*}{\rho g H} \ , \ \ (x,y) = \Big(\frac{\varepsilon^{\frac{1}{2}}x^*}{H}, \frac{y^*}{H}\Big) \ ,$$

$$(u,v) = \Big(\frac{u^*}{\sqrt{gH}}, \frac{\varepsilon^{\frac{1}{2}}v^*}{\sqrt{gH}}\Big) \ , \ \ b(x) = \frac{b^*(x^*)\varepsilon^{-2}}{\rho g H}$$

$\varepsilon = \Big(\frac{H}{L}\Big)^2 \ll 1$ where H and L are horizontal and vertical length scales.

In terms of these non-dimensional quantities, the above equations become

$$u_x + v_y = 0$$

$$uu_x + vu_y = -p_x$$

$$\varepsilon(uv_x + vv_y) = -p_y - 1$$

at $y = -1$; $\qquad\qquad\qquad v = 0$

at $y = \varepsilon\eta$; $\qquad\qquad\quad \varepsilon u\eta_x - v = 0$

$$p = \varepsilon^2 b(x)$$

where $b(x)$ has a compact support.

In the following, we use a unified asymptotic method to derive the equations for $\eta(x)$.

$$(u,v) = (u_0, v_0) + \varepsilon(u_1, v_1) + \varepsilon^2(u_2, v_2) + \mathcal{O}(\varepsilon^3) \tag{1.1}$$

$$p = p_0 + \varepsilon p_1 + \varepsilon^2 p_2 + \mathcal{O}(\varepsilon^3) \tag{1.2}$$

and then expand $p_0, p_1, p_2, ...$ about $y = 0$ with η.

$$p = \Big(p_0 + \varepsilon p_{0y}\eta + \varepsilon^2 p_{0yy}\frac{\eta^2}{2!} + ...\Big) + \varepsilon\Big(p_1 + \varepsilon p_{1y}\eta + \varepsilon^2 p_{1yy}\frac{\eta^2}{2!} + ...\Big)$$

$$+\varepsilon^2\Big(p_2 + \varepsilon p_{2y}\eta + \varepsilon^2 p_{2yy}\frac{\eta^2}{2!} + ...\Big) + \mathcal{O}(\varepsilon^3) \tag{1.3}$$

At $x = -\infty$, we consider $U = 1 + \varepsilon\lambda + \mathcal{O}(\varepsilon^2)$, where $U = \dfrac{U^*}{\sqrt{gH}} = F$.

Substituting (1.1),(1.2) and(1.3) in the above equations to get the zeroth, first and second approximations as follows.

zeroth approximation

$$u_{0x} + v_{0y} = 0$$

$$u_0 u_{0x} + v_0 u_{0y} = -p_{0x}$$

$$-p_{0y} - 1 = 0$$

at $y = -1$; $v_0 = 0$

at $y = 0$; $v_0 = 0$ and $p_0 = 0$.

These imply that $u_0(x, y) = 1$, $v_0(x, y) = 0$ and $p_0(x, y) = -y$.

First approximation

$$u_{1x} + v_{1y} = 0$$

$$u_0 u_{1x} + u_1 u_{0x} + v_0 u_{1y} + v_{1u_{0y}} = -p_{1x}$$

$$u_0 v_{0x} + v_0 v_{0y} = -p_{1y}$$

at $y = -1$; $v_1 = 0$

at $y = \eta$; $p_{0y}\eta + p_1 = 0$.

These imply that $u_1(x, y) = -\eta + \lambda$, $v_1(x, y) = \eta_x(y + 1)$ and $p_1(x, y) = \eta$.

Second approximation

$$u_{2x} + v_{2y} = 0$$

$$u_2 u_{0x} + u_1 u_{1x} + u_0 u_{2x} + v_0 u_{2y} + v_1 u_{1y} + v_2 u_{0y} = -p_{2x}$$

$$u_0 v_{1x} + u_1 v_{0x} + v_0 v_{1y} + v_1 v_{0y} = -p_{2y}$$

at $y = -1$; $v_2 = 0$

at $y = 0$; $p_{0yy}\dfrac{\eta^2}{2} + p_{1y}\eta + p_2 = b(x)$.

These imply that

$$u_{2x}(x, y) = \eta_{xxx}\Big(\frac{y^2}{2} + y\Big) - b_x(x) - \eta\eta_x + \lambda\eta_x$$

$$v_2(x, y) = -\eta_{xxx}\Big(\frac{y^3}{6} + \frac{y^2}{2} - \frac{1}{3}\Big) + (b_x(x) + \eta\eta_x - \lambda\eta_x)(y + 1)$$

$$p_2(x, y) = -\eta_{xx}\Big(\frac{y^2}{2} + y\Big) + b(x).$$

For the kinematic boundary condition at $y = \varepsilon\eta$, $\varepsilon u\eta_x - v = 0$. We expand u, v about $y = 0$ with η as follows.

$$\varepsilon\left[\left(u_0 + \varepsilon u_{0y}\eta + \varepsilon^2 u_{0yy}\frac{\eta^2}{2!} + \ldots\right) + \varepsilon\left(u_1 + \varepsilon u_{1y}\eta + \varepsilon^2 u_{1yy}\frac{\eta^2}{2!} + \ldots\right) + \ldots\right]\eta_x$$
$$-\left[\left(v_0 + \varepsilon v_{0y}\eta + \varepsilon^2 v_{0yy}\frac{\eta^2}{2!} + \ldots\right) + \varepsilon\left(v_1 + \varepsilon v_{1y}\eta + \varepsilon^2 v_{1yy}\frac{\eta^2}{2!} + \ldots\right)\right.$$
$$\left.+\varepsilon^2\left(v_2 + \varepsilon v_{2y}\eta + \varepsilon^2 v_{2yy}\frac{\eta^2}{2!} + \ldots\right) + \ldots\right] = 0.$$

<u>Zeroth approximation</u>

at $y = 0$, $v_0 = 0$.

<u>First approximation</u>

at $y = \eta$, $u_0\eta_x - v_{0y}\eta - v_1 = 0$.

That is $\eta_x - v_1 = 0$.

<u>Second approximation</u>

at $y = 0$, $(u_{0y}\eta + u_1)\eta_x - \left(v_{0yy}\frac{\eta^2}{2} + \eta v_{1y} + v_2\right) = 0$.

That is

$$3\eta\eta_x - 2\lambda\eta_x + \frac{1}{3}\eta_{xxx} + b_x(x) = 0 \qquad (1.4)$$

which is called a forced stationary Korteweg-de Vries equation.

We consider now that the distribution of pressure be described by function with compact support defined by

$$b(x) = \begin{cases} 0 & \text{for } |x| \geq 1 \\[2mm] \epsilon\exp\left(\dfrac{1}{x^2 - 1}\right) & \text{for } |x| < 1 \end{cases}$$

where ϵ is a constant.

In this research, we will state and prove theorems to guarantee the existence of solutions of (1.4). We consider two separate cases according to the characteristic of the solution. The first case is when $\lambda > 0$ (supercritical flow) and the other is $\lambda < 0$ (subcritical flow). Numerical solutions for both cases are obtained by the shooting method and the Runge-Kutta method, respectively. In the case of

supercritical flow, our numerical results show that the flow is always symmetric (drag free) with respect to the axis of symmetry of the pressure distribution. There are two different families of solutions when $\epsilon > 0$. One family is a perturbed solution of uniform stream whereas the other is a perturbed solution of solitary wave. When $\epsilon < 0$, there exists only one family of solutions for all values of λ up to zero. We expect that these solution can be extended to the subcritical regime by allowing waves downstream. The case of subcritical flow, a train of nonlinear waves is generated behind the applied pressure distribution while the flow satisfies the radiation condition on the upstream. As λ decreases, there are critical values of λ at which the flows become drag free. Our finding is in contrast with the problem of flows past a surface-piercing object. Asavanant and Vanden-Broeck (1994) showed that subcritical flows past a parabolic-shaped object never possess drag-free solutions. On the contrary, these solutions always approach Stokes' limiting configuration.

CHAPTER II

Supercritical Flow

2.1 Existence Theorem of Symmetric Solutions

We look for a solution $\eta(x)$ of (1.4) such that $\lim\limits_{|x|\to\infty} \left(\dfrac{d}{dx}\right)^j \eta(x) = 0$, $j = 0, 1, 2$,
where $\lambda > 0$.

Integrating (1.4) from $-\infty$ to x, we find

$$6\lambda\eta - \eta_{xx} = \frac{9}{2}\eta^2 + 3b(x). \tag{2.1}$$

It can easily be shown that the above equation is equivalent to an integral
equation

$$\eta(x) = \int_{-\infty}^{\infty} K(x,\xi)\left(\frac{9}{2}\eta^2(\xi) + 3b(\xi)\right)d\xi.$$

Here $K(x,\xi) = \dfrac{e^{-\sqrt{6\lambda}|x-\xi|}}{2\sqrt{6\lambda}}$ is the Green's function which is a solution of

$$6\lambda K(x,\xi) - K_{xx}(x,\xi) = \delta(x - \xi), -\infty < x, \xi < \infty.$$

We now define

$$T(\eta) = \int_{-\infty}^{\infty} K(x,\xi)\left(\frac{9}{2}\eta^2(\xi) + 3b(\xi)\right)d\xi.$$

$$\|u\| = \|u\|_\infty = \sup_{x\in\mathbb{R}} |u(x)|$$

$$H = \{u|u \in C(\mathbb{R}); \|e^{\sqrt{6\lambda}|x|}u\| < \infty\}.$$

Clearly, H is a metric space and is complete. We give another definition

$$B_M = \{u|u \in H\,, \|u\| \le M,\ \ 0 < M < \infty\}.$$

Lemma 2.1 $\|T(\eta)\| \le M$ for $\eta \in B_M$ if $\dfrac{9}{2}M + \dfrac{3\|b\|}{M} \le 6\lambda$.

Proof
$$
\begin{aligned}
\|T(\eta)\| &= \sup_{x \in \mathbb{R}} \Big| \int_{-\infty}^{\infty} K(x,\xi)\Big(\frac{9}{2}\eta^2(\xi) + 3b(\xi)\Big)d\xi \Big| \\
&\le \Big\| \frac{9}{2}\eta^2 + 3b \Big\| \sup_{x \in \mathbb{R}} \int_{-\infty}^{\infty} \frac{1}{2\sqrt{6\lambda}} e^{-\sqrt{6\lambda}|x-\xi|} d\xi \\
&\le \frac{(\frac{9}{2}M^2 + 3\|b\|)}{6\lambda} \\
&\le M
\end{aligned}
$$

as required.

$\square$

Next we want to prove that $T(\eta)$ decays rapidly so that we may consider the behavior of $\exp(\sqrt{6\lambda}|x|)|T(\eta)(x)|$ when $|x|$ is large.

Lemma 2.2 $\displaystyle \sup_{x \in \mathbb{R}} \exp(\sqrt{6\lambda}|x|)|T(\eta)(x)| < \infty$ for $\eta \in B_M$.

Proof It suffices to prove the case when $x > 0$.

$$
\begin{aligned}
e^{\sqrt{6\lambda}|x|}|T(\eta)(x)| &= \Big| \int_{-\infty}^{\infty} \exp(\sqrt{6\lambda}x - \sqrt{6\lambda}|x-\xi|)\Big(\frac{9}{2}\eta^2(\xi) + 3b(\xi)\Big)d\xi \Big| \Big/ 2\sqrt{6\lambda} \\
&= \Big| \int_{-\infty}^{x} \exp(\sqrt{6\lambda}\xi)\Big(\frac{9}{2}\eta^2(\xi) + 3b(\xi)\Big)d\xi \\
&\quad + \int_{x}^{\infty} \exp(\sqrt{6\lambda}(2x-\xi))\Big(\frac{9}{2}\eta^2(\xi) + 3b(\xi)\Big)d\xi \Big| \Big/ 2\sqrt{6\lambda} \\
&= \Big| \int_{-\infty}^{x} \Big\{ \frac{9}{2}\exp(\sqrt{6\lambda}\xi - 2\sqrt{6\lambda}|\xi|)(\eta(\xi)\exp(\sqrt{6\lambda}|\xi|))^2 \\
&\quad + \exp(\sqrt{6\lambda}\xi)3b(\xi) \Big\}d\xi \\
&\quad + \int_{x}^{\infty} \Big\{ \frac{9}{2}\exp(\sqrt{6\lambda}(2x-\xi) - 2\sqrt{6\lambda}|\xi|)(\eta(\xi)\exp(\sqrt{6\lambda}|\xi|))^2 \\
&\quad + 3b(\xi)\exp(\sqrt{6\lambda}(2x-\xi)) \Big\}d\xi \Big| \Big/ 2\sqrt{6\lambda} \\
&\le \Big| \sup_{x \in \mathbb{R}}(\eta(x)\exp(\sqrt{6\lambda}|x|))^2 \Big[\int_{-\infty}^{x} \exp(-\sqrt{6\lambda}|\xi|)d\xi \\
&\quad + \int_{x}^{\infty} \exp(\sqrt{6\lambda}(2x-3\xi))d\xi \Big] \Big| \frac{9}{4\sqrt{6\lambda}} \\
&\quad + \Big| \int_{-\infty}^{x} \exp(\sqrt{6\lambda}\xi)3b(\xi)d\xi \\
&\quad + \int_{x}^{\infty} 3b(\xi)\exp(\sqrt{6\lambda}(2x-\xi))d\xi \Big| \Big/ 2\sqrt{6\lambda}
\end{aligned}
$$

$$\leq \frac{3}{4\lambda}\Big|\Big(1 - \frac{\exp(-\sqrt{6\lambda}x)}{3}\Big)\Big| \sup_{x\in\mathbb{R}}(\eta(x)\exp(\sqrt{6\lambda}|x|))^2$$
$$+ \int_{supp(b(x))} N\exp(\sqrt{6\lambda}\xi)d\xi\Big/ 2\sqrt{6\lambda}$$
$$< \infty,$$

where $N = \max\limits_{\xi\in\mathbb{R}}|3b(\xi)|$. Since $\eta \in H$,

$$\sup_{x>0}\exp(\sqrt{6\lambda}x)|T(\eta)(x)| < \infty.$$

Similarly, one can easily show that

$$\sup_{x<0}\exp(-\sqrt{6\lambda}x)|T(\eta)(x)| < \infty.$$

This completes the proof.

$\square$

Now we shall states the existence theorem for symmetric solutions of (2.1).

Theorem 2.1 $6\lambda\eta - \eta_{xx} = \dfrac{9}{2}\eta^2 + 3b(x), \quad -\infty < x < \infty$ has a solution

which decays exponentially at $|x| = \infty$ if 6λ is sufficiently large.

Proof.
$$\|T(\eta_1) - T(\eta_2)\| \leq \sup_{x\in\mathbb{R}}\Big|\frac{9}{2}\int_{-\infty}^{\infty} K(x,\xi)(\eta_1^2(\xi) - \eta_2^2(\xi))d\xi\Big|$$
$$\leq \sup_{x\in\mathbb{R}}\frac{9}{2}\int_{-\infty}^{\infty} K(x,\xi)|\eta_1 + \eta_2||\eta_1 - \eta_2|d\xi$$
$$\leq 9M\|\eta_1 - \eta_2\|\Big/ 6\lambda.$$

Hence we can see from lemma 2.1 and 2.2 that T is a contraction mapping if

$6\lambda > \max\Big\{\dfrac{9}{2}M + \dfrac{3\|b\|}{M}, 9M\Big\}$ and the integral equation $\eta = T(\eta)$ has the unique

solution in B_M. Now

$$\eta_{xx} = \int_{-\infty}^{\infty} K_{xx}(x,\xi)\Big(\frac{9}{2}\eta^2(\xi) + 3b(\xi)\Big)d\xi$$

$$= \int_{-\infty}^{\infty} 6\lambda K(x,\xi)\Big(\frac{9}{2}\eta^2(\xi) + 3b(\xi)\Big)d\xi - \frac{9}{2}\eta^2(x) - 3b(x)$$
$$= 6\lambda\eta(x) - \frac{9}{2}\eta^2(x) - 3b(x)$$

where $6\lambda K(x,\xi) - K_{xx}(x,\xi) = \delta(x - \xi)$. Hence $\eta \in C^2(\mathbb{R})$ and it follows from

right hand side of the above equation that $\eta \in C^3(\mathbb{R})$.

$\square$

2.2   Numerical Procedure

To obtain weakly nonlinear solutions of (2.1) in the previous section, it is necessary to resort to a numerical method. We solve this boundary value problem by the method of shooting. Here is the general idea of this method.

Suppose that we have a similar problem, which we are unable to determine the general solution as in (2.1), for example

$$x''(t) = f(t, x(t), x'(t)) \quad ; \quad x(a) = \alpha \; , x(b) = \beta \tag{2.2}$$

the approach is to view (2.2) as an initial value problem. A step-by-step numerical solution of problem (2.2) then by the method of Runge-Kutta 4th order (RK4) requires two initial conditions. But in problem (2.2), only one condition is presented at $t = a$. One way to proceed in solving equation (2.2) is as follows: guess $x'(a)$ and carry out the calculations with the hope that the computed solution agrees with $x(b) = \beta$. If it is missed (which is quite likely), we can go back and change our guess for $x'(a)$. Repeating this procedure until we hit the target β. This briefly describes the shooting procedure.

In this research, we solve the equation (2.1) by discretizing the free surface in the physical plane, $x \in [-1, 1]$. The value of $\eta(x)$ are computed at each mesh points. As a summary, a function $\eta(x)$ is computed as follows :

   (i) set the initial condition $\eta(-1)$,

   (ii) guess the first initial slope, $\eta'(-1)$,

   (iii) use system of RK4 to get the first value of $\eta(1)$ and find the error at the

boundary condition,

(iv) guess the second initial slope at $x = -1$ (related with the first initial guess),

(v) use system of RK4 again to obtain the value of $\eta(1)$, then check the error at the boundary and go back to step (ii), adjust our guess until the solution converges.

To compute the numerical solution of this problem, we divide it into two cases. The first is for the positive pressure ($\epsilon > 0$), there are two different types of solution. So, we have to set two different boundary conditions which will be mentioned later. The second is for the negative pressure ($\epsilon < 0$). The numerical results for every cases will be shown and discussed in the next section.

2.3 Numerical Results and Discussions

We use the numerical scheme described in the previous section to compute symmetric solutions in supercritical flow regime for various values of $\lambda > 0$ and ϵ. It is found that supercritical solutions are characterized by exponentially decaying behavior at infinity. This means that solutions in this flow regime can never possess downstream waveforms.

It can be seen from equation (1.4) that if $b(x) = 0$ (i.e. pressure on the free surface equals to atmospheric pressure), then uniform flow is always a solution for all values of $\lambda > 0$. Besides uniform flow solution, one can also find another solution namely *solitary wave* solution. The exact expression of solitary wave solution can be derived from the weakly nonlinear analysis as

$$\eta(x) = 2\lambda \text{sech}^2\left(\sqrt{\frac{3\lambda}{2}}x\right), \quad -\infty < x < \infty, \text{(as shown in Figure 2.1 for } \lambda = 1\text{)}.$$

It bifurcates from the uniform flow at the critical Froude number $F^2 = 1$ ($\lambda = 0$).

It is anticipated that solutions of free-surface flow due to pressure distribution ($\epsilon \neq 0$) is the perturbation of a uniform stream solution since uniform flow is no longer a solution for any values of λ when $\epsilon \neq 0$. Also we expect to obtain a perturbed bifurcation of solitary wave solution. To discuss the numerical calculations of such supercritical flow solutions, we consider 2 cases : $\epsilon > 0$ (positive pressure) and $\epsilon < 0$ (negative pressure). The solutions are characterized by a dimensionless distance W measured from the undisturbed level of the free surface to the maximum (or minimum) elevation on the free surface profile upon which the pressure distribution is applied.

(i) Positive pressure

When $\epsilon > 0$, there are two types of solution that characterized by $W > 0$. One can be viewed as perturbation of uniform stream (Type I, see Figure 2.2). The other is the perturbation of solitary wave solution (Type II, see Figure 2.3). To obtain the profiles of Type I, we use the boundary condition with phase shift x_0, that is

$$\eta(-1) = 2\lambda\text{sech}^2\Big(\sqrt{\frac{3\lambda}{2}}(-1 - x_0)\Big) \quad , \quad \eta(1) = 2\lambda\text{sech}^2\Big(\sqrt{\frac{3\lambda}{2}}(1 + x_0)\Big).$$

Let $\eta'(-1^-)$ be the slope of η that we determine at the boundary $x = -1$ and $\eta'(-1^+)$ be the numerical slope of η that we calculate from the shooting method. We vary x_0 and use the shooting method until the convergence is achieved and

$$|\eta'(-1^-) - \eta'(-1^+)| < 10^{-3}.$$

While, we use the boundary condition without a phase shift, i.e.

$$\eta(-1) = 2\lambda\text{sech}^2\Big(-\sqrt{\frac{3\lambda}{2}}\Big) \quad , \quad \eta(1) = 2\lambda\text{sech}^2\Big(\sqrt{\frac{3\lambda}{2}}\Big),$$

to calculate the free surface profiles of Type II solution. Figure 2.4 shows a comparison of flow profiles at the same value of λ. The numerical values of λ

versus W for various values of ϵ are presented in Figure 2.5. As we can see, there are two branches of solution for each ϵ and λ. The lower branch (closer to the λ-axis) is the Type I solution while the upper branch (farther away from the λ-axis) is the Type II solution.

Consider Type I solution. Figure 2.6 shows that, for λ fixed, the magnitude of pressure induces higher amplitude W as ϵ increases. On the other hand, Figure 2.7 shows that W decreases as ϵ increases for the Type II solution. The differences between the shape of free-surface profiles between Type I and II solutions are depicted in Figure 2.8 and 2.9, respectively. As we can see, for the Type I solution, W decreases for increasing value of λ when we fix ϵ. Unlike Type I solution, we can notice that, W increases for increasing value of λ when we fix ϵ in the case of Type II solution. The relationships between λ and W for the Type I and Type II solutions are presented in Figure 2.10 and 2.11, respectively.

(ii) Negative pressure

When $\epsilon < 0$, there exists a unique solution corresponding to each value of λ when $0 \leq \lambda < \infty$. This solution can be viewed as perturbation of a uniform flow (i.e. they approach the uniform stream as $\epsilon \to 0$ for a fixed value of λ). Typical free-surface profiles for $\epsilon < 0$ are shown in Figure 2.12 and 2.13. Here, the free surface profiles are calculated by using the boundary condition with a phase shift x_0. We first set an initial slope in the opposite sign of the case of positive pressure, that is

$$\eta(-1) = -2\lambda \text{sech}^2\left(\sqrt{\frac{3\lambda}{2}}(-1 - x_0)\right) \quad , \quad \eta(1) = -2\lambda \text{sech}^2\left(\sqrt{\frac{3\lambda}{2}}(1 + x_0)\right),$$

then varying x_0 until the loop of shooting converges and the slope $\eta'(-1^-)$ and $\eta'(-1^+)$ satisfy the above criteria. Numerical values of λ versus W for various value of ϵ are presented in Figure 2.14. We expect that these branches of solutions can be extended to the subcritical regime ($\lambda < 0$) by allowing waves downstream.

Solutions with waves will be considered in the next chapter.
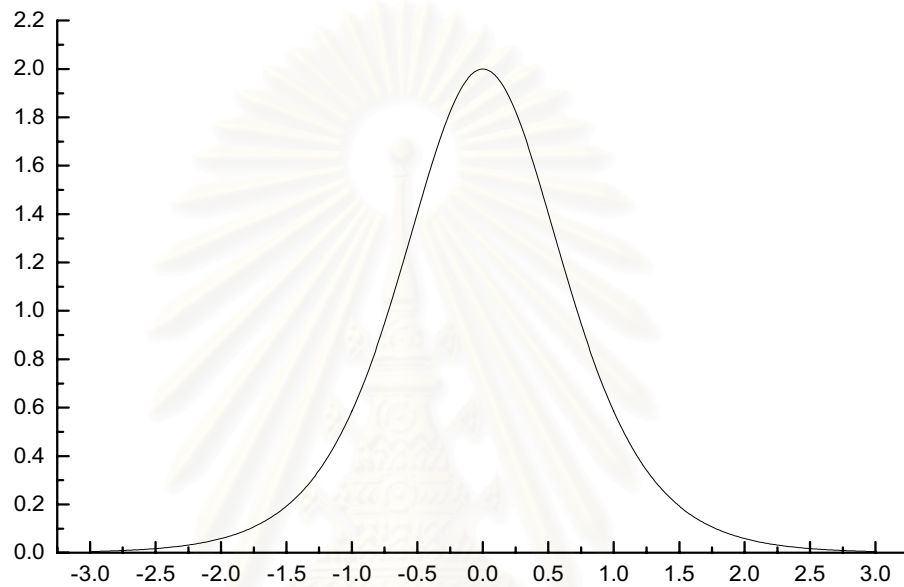
Figure 2.1: Typical free-surface profile for $\lambda = 1$ and $\epsilon = 0$.
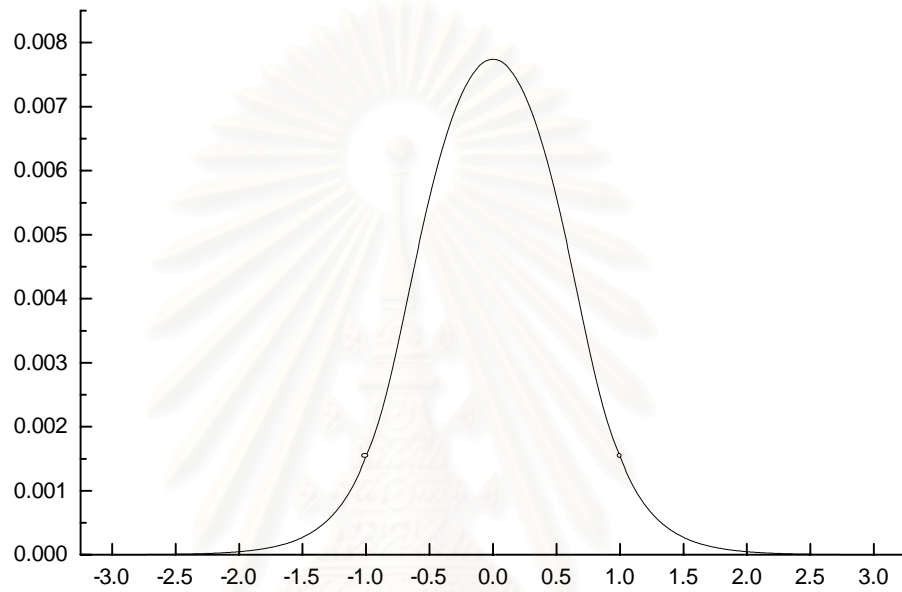
Figure 2.2: Typical free-surface profile of Type I for $\lambda = 2$ and $\epsilon = 0.1$.
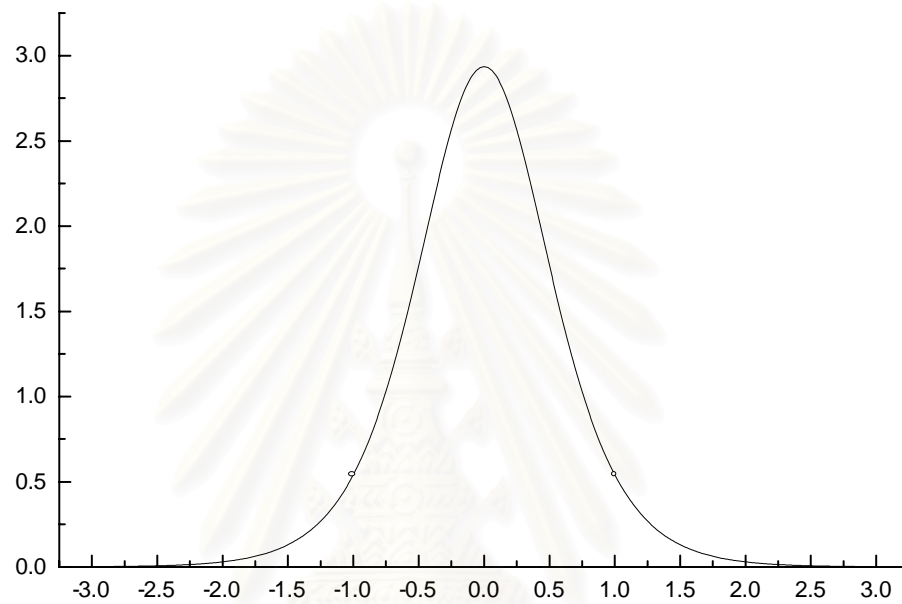
Figure 2.3: Typical free-surface profile of Type II for $\lambda = 1.5$ and $\epsilon = 0.5$.
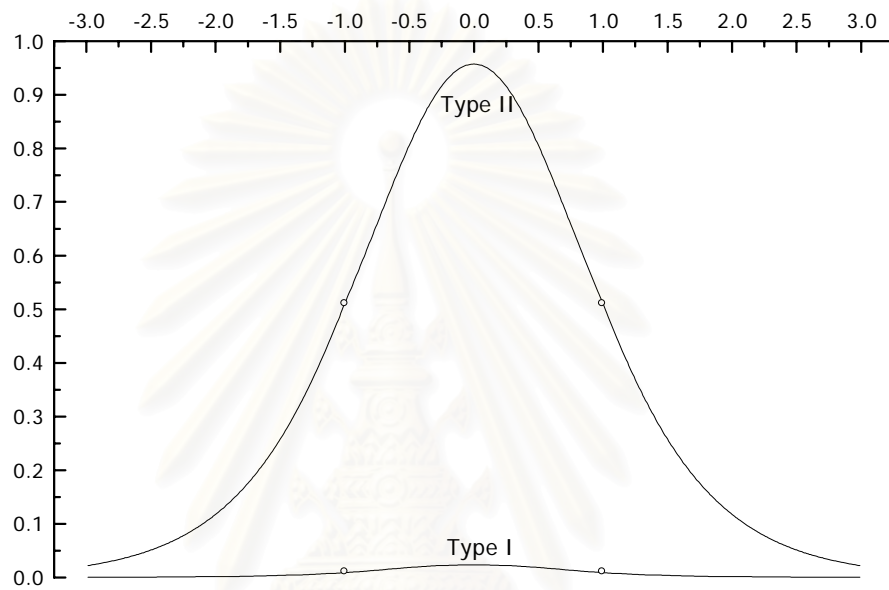
Figure 2.4: Typical free-surface profile of Type I and Type II for $\lambda = 0.5$ and $\epsilon = 0.1$.
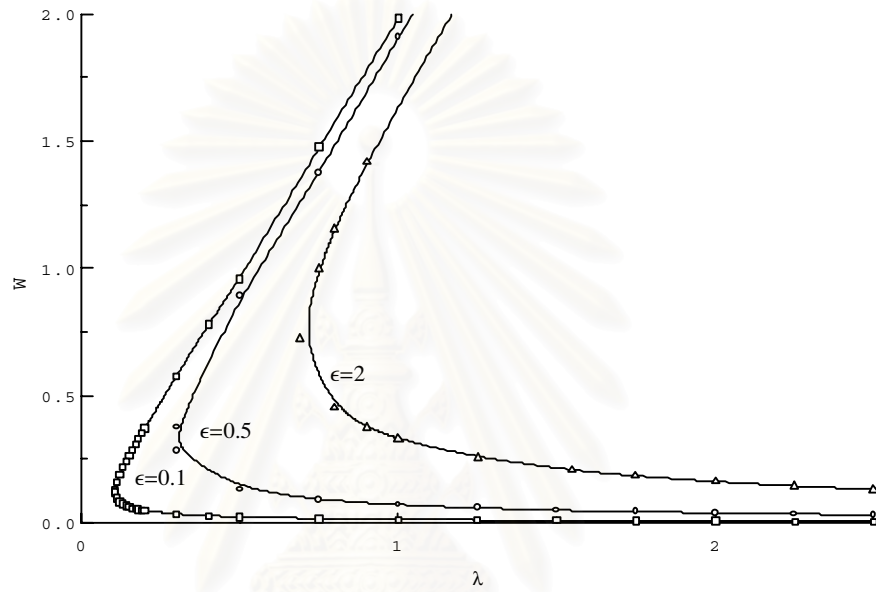
Figure 2.5: Relationship between W and λ for various values of $\epsilon > 0$.
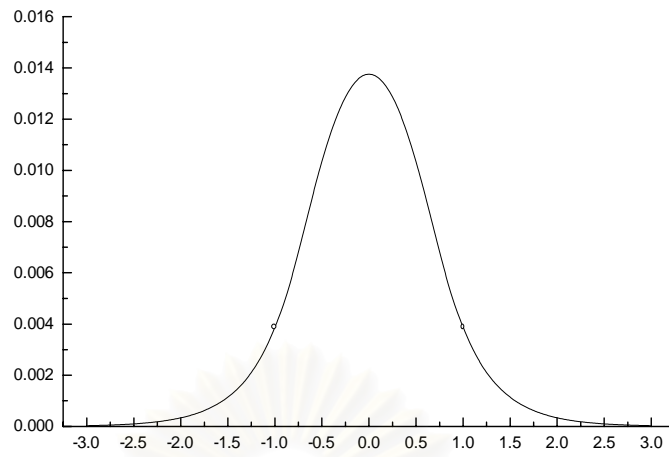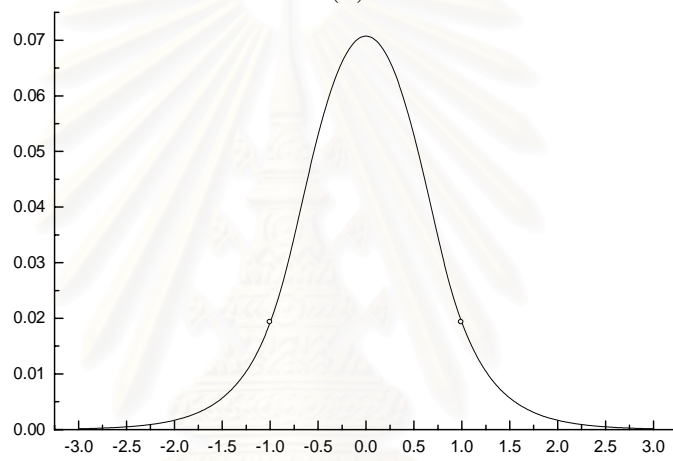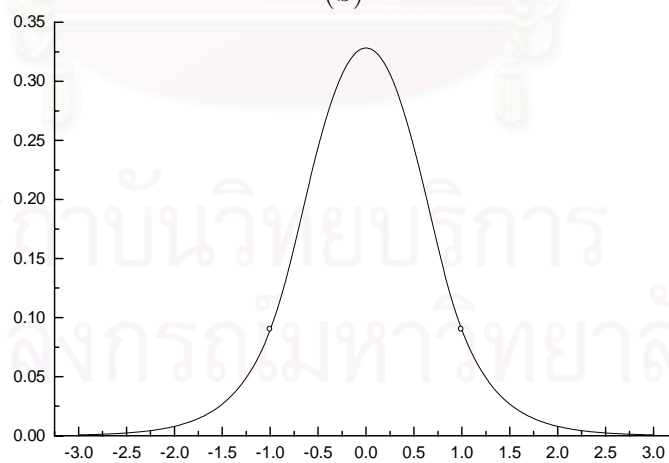
Figure 2.6: Typical free-surface profiles of Type I (a) for $\lambda = 1$, $\epsilon = 0.1$, (b) for $\lambda = 1$, $\epsilon = 0.5$, and (c) for $\lambda = 1$, $\epsilon = 2$.
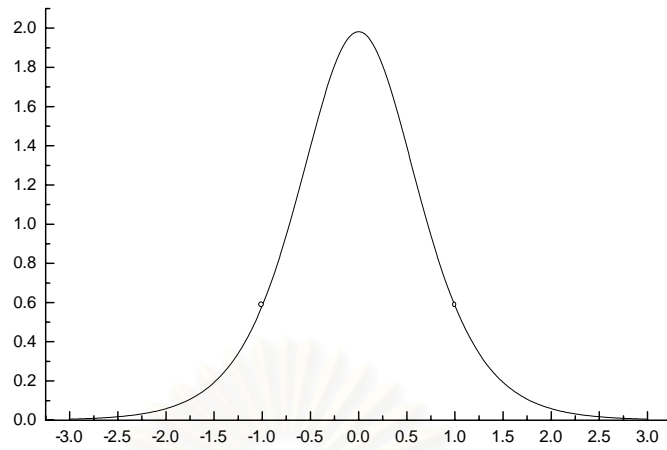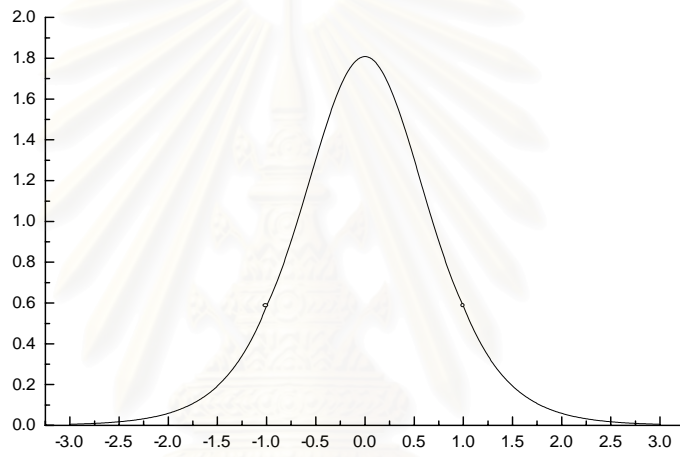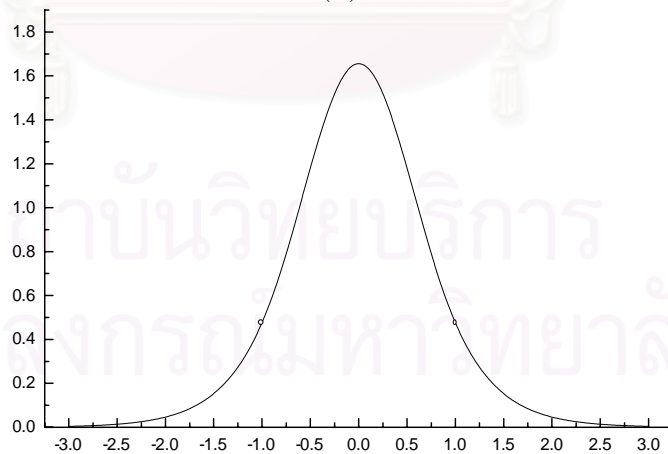
Figure 2.7: Typical free-surface profiles of Type II (a) for $\lambda = 1$, $\epsilon = 0.1$, (b) for $\lambda = 1$, $\epsilon = 1$, and (c) for $\lambda = 1$, $\epsilon = 2$.
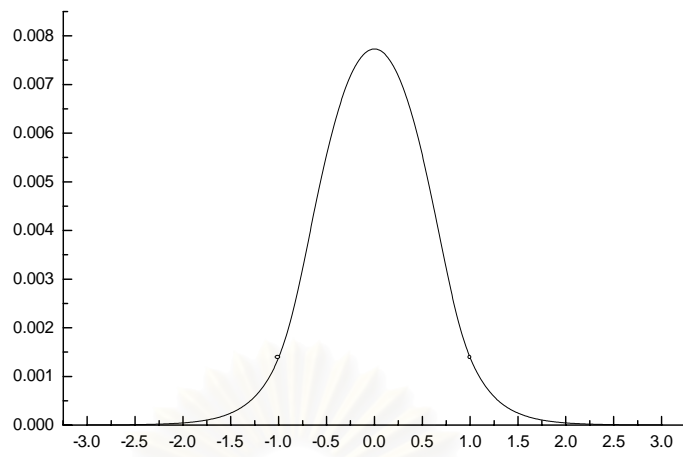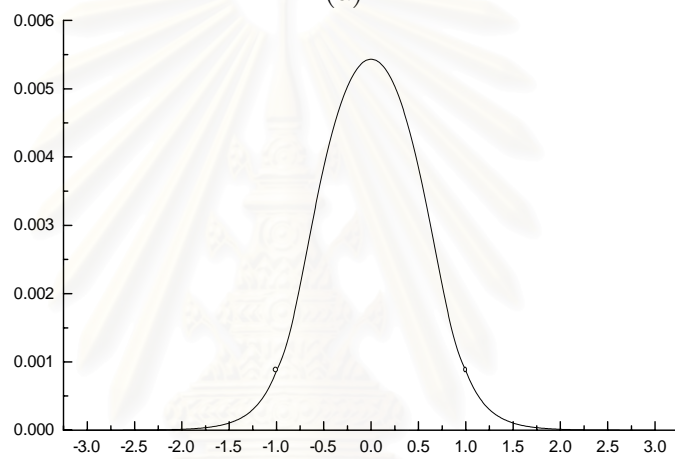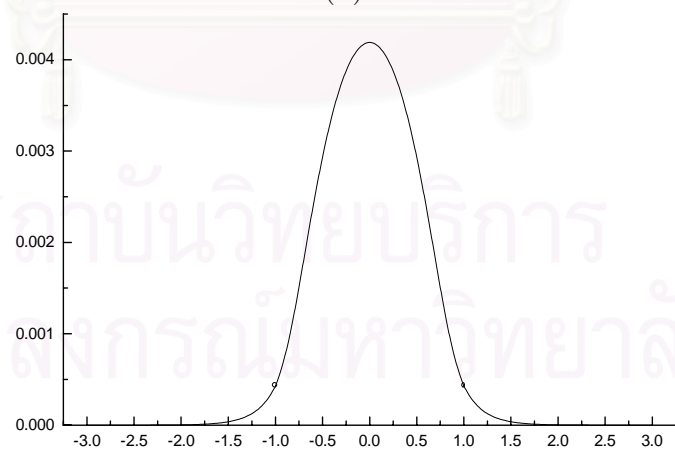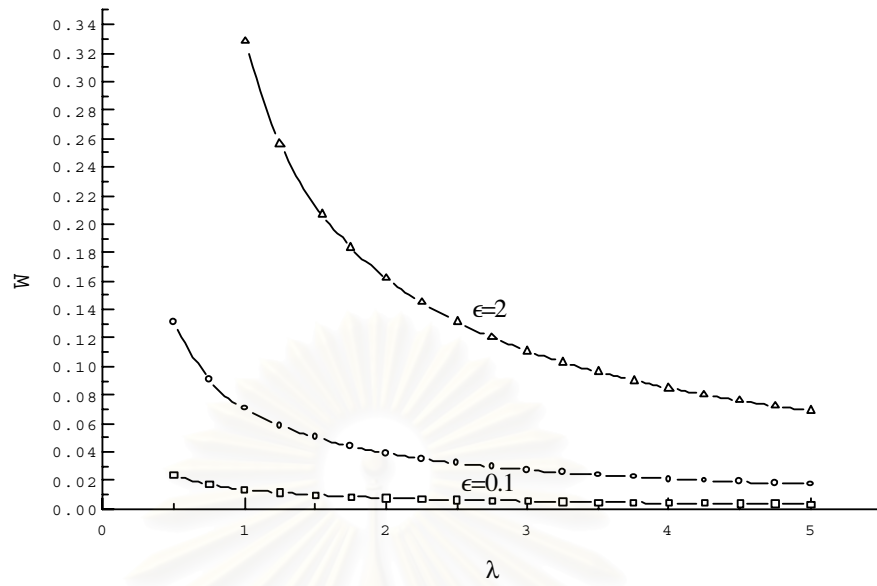
Figure 2.8: Typical free-surface profiles of Type I (a) for $\lambda = 2$, $\epsilon = 0.1$, (b) for $\lambda = 3$, $\epsilon = 0.1$, and (c) for $\lambda = 4$, $\epsilon = 0.1$.
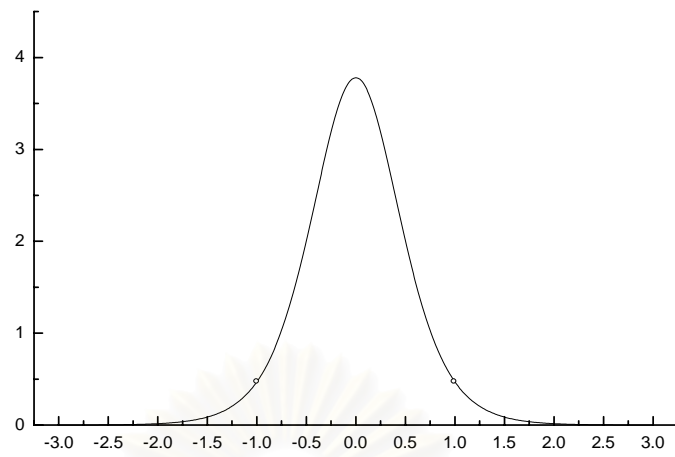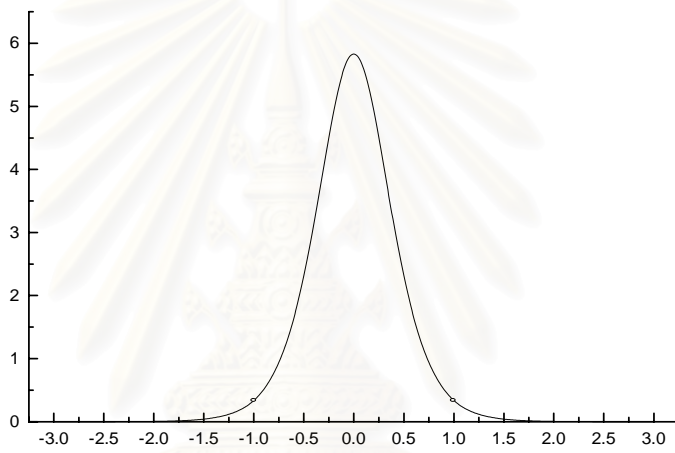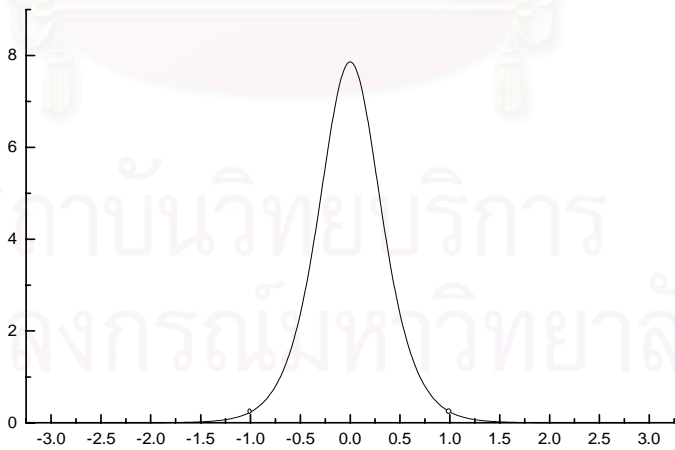
Figure 2.9: Typical free-surface profiles of Type II (a) for $\lambda = 2$, $\epsilon = 2$, (b) for $\lambda = 3$, $\epsilon = 2$, and (c) for $\lambda = 4$, $\epsilon = 2$.

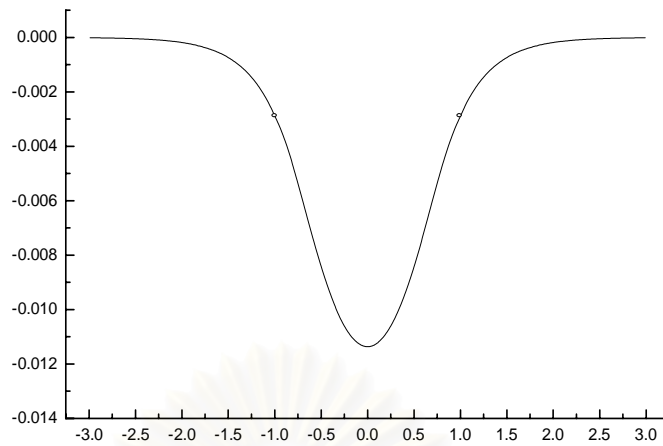Figure 2.10: Relationship between W and λ of Type I solutions for various values of $\epsilon > 0$.
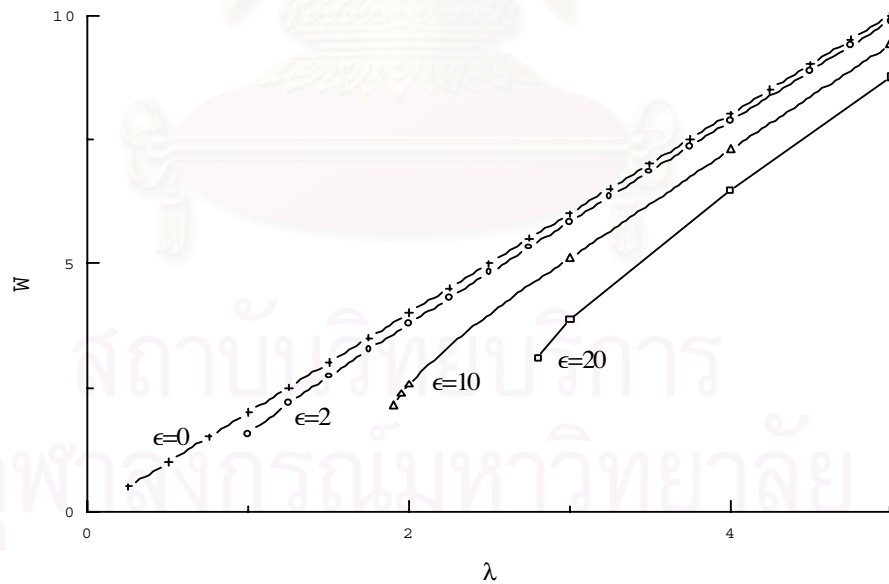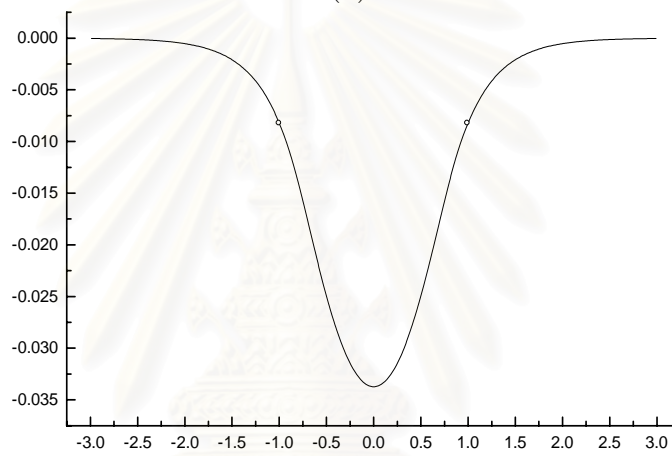

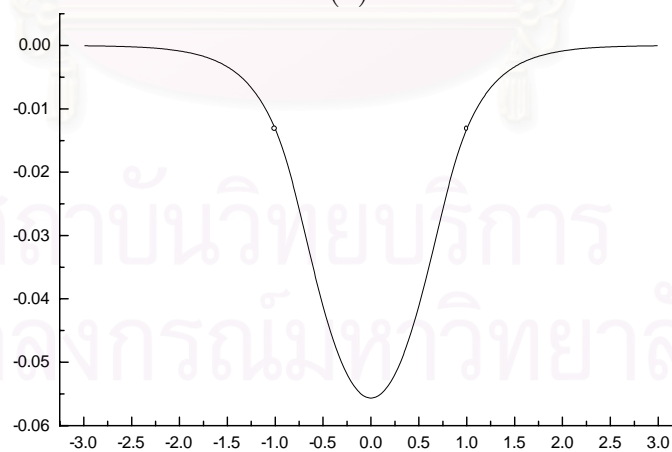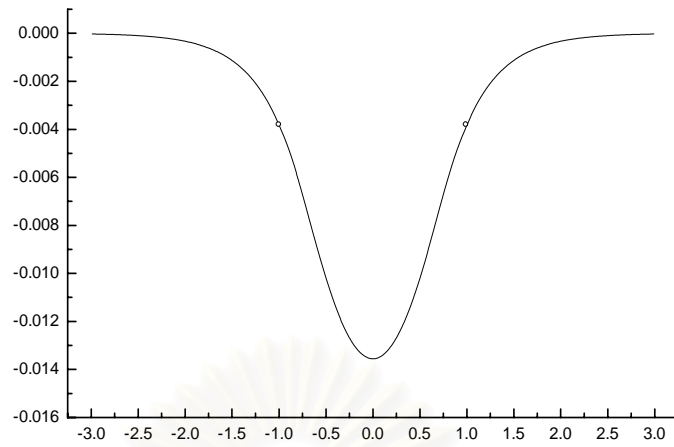Figure 2.11: Relationship between W and λ of Type II solutions for various values of $\epsilon > 0$.

Figure 2.12: Typical free-surface profiles (a) for $\lambda = 1.25$, $\epsilon = -0.1$, (b) for $\lambda = 1.25$, $\epsilon = -0.3$, and (c) for $\lambda = 1.25$, $\epsilon = -0.5$.

(a)

(b)
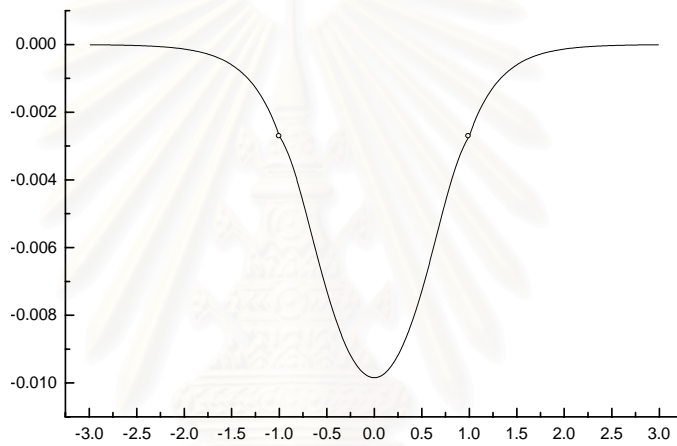

(c)
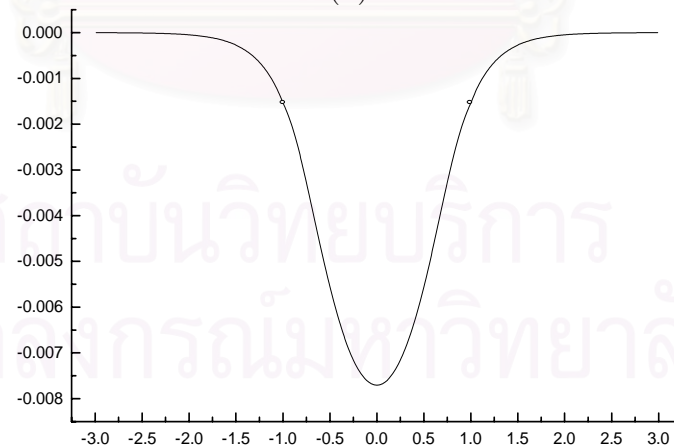
Figure 2.13: Typical free-surface profiles (a) for $\lambda = 1$, $\epsilon = -0.1$, (b) for $\lambda = 1.5$, $\epsilon = -0.1$, and (c) for $\lambda = 2$, $\epsilon = -0.1$.
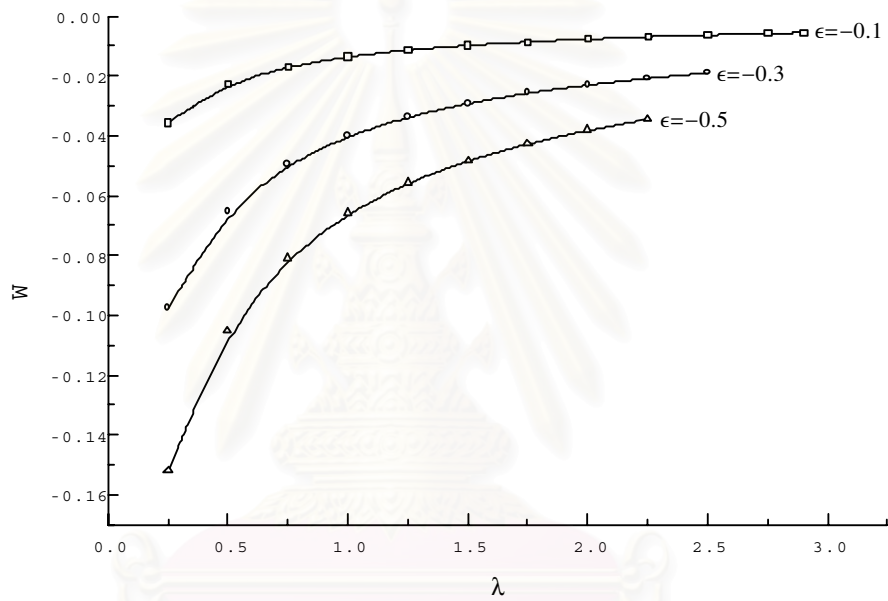
Figure 2.14: Relationship between W and λ for various values of $\epsilon < 0$.

CHAPTER III

Subcritical Flow

3.1 Existence Theorem of Unsymmetric Solutions

Consider

$$\eta_{xx} + \frac{9}{2}\eta^2 - 6\lambda\eta = -3b(x). \tag{3.1}$$

For subcritical $\lambda < 0$, say $\lambda_0 = -\lambda$ where $\lambda_0 > 0$,

(3.1) becomes

$$\eta_{xx} + \frac{9}{2}\eta^2 + 6\lambda_0\eta = -3b(x). \tag{3.2}$$

We look for a wave solution to equation (3.2), for $\lambda < 0$, which dies out at the far upstream and oscillates without changing its amplitude at the far downstream. That is to say, η must satisfy the followings:

(i) $\dfrac{d^i\eta}{dx^i} = 0$, $i = 0, 1, 2$ for $x < x_- = \inf(supp\ b)$.

(ii) $\eta\left(x + \dfrac{2\pi}{\sqrt{6\lambda_0}}\right) = \eta(x)$ for $x > x_+ = \sup(supp\ b)$.

Without loss of generality we assume that $supp(b) \cap \mathbb{R}^- = \phi$.

It can easily be shown that (3.2) is equivalent to an integral equation

$$\eta(x) = \begin{cases} 0 & ; x \le 0 \\ -\dfrac{1}{\sqrt{6\lambda_0}}\displaystyle\int_0^x \sin\sqrt{6\lambda_0}(x-\xi)\left[\dfrac{9}{2}\eta^2(\xi) + 3b(\xi)\right]d\xi & ; x > 0. \end{cases}$$

We now define $\eta = S(\eta)$,

$$B = \left\{ u \middle| u \in C(\mathbb{R}), \quad u(x) = 0 \text{ for } x \le 0 \text{ and } u\left(x + \frac{2\pi}{\sqrt{6\lambda_0}}\right) = u(x) \right.$$

$$\left. \text{and } \int_x^{x+\frac{2\pi}{\sqrt{6\lambda}}} u^2(\xi)\{\sin, \cos\}(\sqrt{6\lambda_0}\xi)d\xi = 0 \text{ for } x > x_+ \right\}$$

$$\|u\| = \sup_{x \in \mathbb{R}} |u(x)|.$$

Clearly, B is a metric space and is complete. We give another definition

$$B_N = \{u | u \in B, \|u\| \le N, \ 0 < N < \infty\}$$

which is a closed subset of B.

Lemma 3.1 $\|S(\eta)\| \le N$ for $\eta \in B_N$ if $\dfrac{9}{2}N\left(x_+ + \dfrac{2\pi}{\sqrt{6\lambda_0}}\right) + \dfrac{3\|b\|}{N}x_+ \le \sqrt{6\lambda_0}$.

Proof $\|S(\eta)\| = \sup\limits_{x \in \mathbb{R}} \left| -\dfrac{1}{\sqrt{6\lambda_0}} \displaystyle\int_0^x \sin\sqrt{6\lambda_0}(x-\xi)\left[\dfrac{9}{2}\eta^2(\xi) + 3b(\xi)\right]d\xi \right|$

$\displaystyle = \frac{1}{\sqrt{6\lambda_0}} \sup_{x \in \mathbb{R}} \Bigg| \int_0^{x_+} \sin\sqrt{6\lambda_0}(x-\xi)\left[\frac{9}{2}\eta^2(\xi) + 3b(\xi)\right]d\xi$

$\displaystyle \qquad + \int_{x_+}^{x_+ + \frac{2\pi}{\sqrt{6\lambda_0}}} \sin\sqrt{6\lambda_0}(x-\xi)\left(\frac{9}{2}\eta^2(\xi)\right)d\xi$

$\displaystyle \qquad + \int_{x_+ + \frac{2\pi}{\sqrt{6\lambda}}}^{x} \sin\sqrt{6\lambda_0}(x-\xi)\left(\frac{9}{2}\eta^2(\xi)\right)d\xi \Bigg|$

$\displaystyle \le \frac{1}{\sqrt{6\lambda_0}} \sup_{x \in \mathbb{R}} \Bigg\{ \left| \int_0^{x_+} \sin\sqrt{6\lambda_0}(x-\xi)\left[\frac{9}{2}\eta^2(\xi) + 3b(\xi)\right]d\xi \right|$

$\displaystyle \qquad + \left| \int_{x_+}^{x_+ + \frac{2\pi}{\sqrt{6\lambda_0}}} \sin\sqrt{6\lambda_0}(x-\xi)\left(\frac{9}{2}\eta^2(\xi)\right)d\xi \right|$

$\displaystyle \qquad + \left| \int_{x_+ + \frac{2\pi}{\sqrt{6\lambda_0}}}^{x_+ + \frac{2\pi n}{\sqrt{6\lambda_0}}} \sin\sqrt{6\lambda_0}(x-\xi)\left(\frac{9}{2}\eta^2(\xi)\right)d\xi \right| \Bigg\} \quad \text{for some } n \in \mathbb{N}$

$\displaystyle \le \frac{1}{\sqrt{6\lambda_0}} \Bigg\{ \left\|\frac{9}{2}\eta^2 + 3b\right\| \sup_{x \in \mathbb{R}} \int_0^{x_+} |\sin\sqrt{6\lambda_0}(x-\xi)|d\xi$

$\displaystyle \qquad + \left\|\frac{9}{2}\eta^2\right\| \sup_{x \in \mathbb{R}} \int_{x_+}^{x_+ + \frac{2\pi}{\sqrt{6\lambda_0}}} |\sin\sqrt{6\lambda_0}(x-\xi)|d\xi \Bigg\}$

$\displaystyle \le \frac{1}{\sqrt{6\lambda_0}} \left\{ \left[\frac{9}{2}N^2 + 3\|b\|\right]x_+ + \frac{9}{2}N^2\frac{2\pi}{\sqrt{6\lambda_0}} \right\}$

$\le N.$

$\square$

Lemma 3.2 If $x > x_+$, then $S(\eta)\Big(x + \dfrac{2\pi}{\sqrt{6\lambda_0}}\Big) = S(\eta)(x)$.

Proof Let $x > x_+$.

$$S(\eta)\Big(x + \frac{2\pi}{\sqrt{6\lambda_0}}\Big) = -\frac{1}{\sqrt{6\lambda_0}} \int_0^{x + \frac{2\pi}{\sqrt{6\lambda_0}}} \sin\sqrt{6\lambda_0}\Big(x + \frac{2\pi}{\sqrt{6\lambda_0}} - \xi\Big)\Big[\frac{9}{2}\eta^2(\xi) + 3b(\xi)\Big]d\xi$$

$$= -\frac{1}{\sqrt{6\lambda_0}} \int_0^{x + \frac{2\pi}{\sqrt{6\lambda_0}}} \sin\sqrt{6\lambda_0}(x - \xi)\Big[\frac{9}{2}\eta^2(\xi) + 3b(\xi)\Big]d\xi$$

$$= -\frac{1}{\sqrt{6\lambda_0}}\Big\{\int_0^{x} \sin\sqrt{6\lambda_0}(x - \xi)\Big[\frac{9}{2}\eta^2(\xi) + 3b(\xi)\Big]d\xi$$

$$+ \int_x^{x + \frac{2\pi}{\sqrt{6\lambda_0}}} \sin\sqrt{6\lambda_0}(x - \xi)\Big(\frac{9}{2}\eta^2(\xi)\Big)d\xi\Big\}$$

$$= S(\eta)(x) - \frac{1}{\sqrt{6\lambda_0}}\int_{-\frac{\pi}{\sqrt{6\lambda_0}}}^{\frac{\pi}{\sqrt{6\lambda_0}}} \sin\sqrt{6\lambda_0}(x - \xi)$$

$$\Big(\frac{9}{2}\eta^2(\xi)\Big)d\Big(\xi - x - \frac{\pi}{\sqrt{6\lambda_0}}\Big)$$

$$= S(\eta)(x).$$

$\square$

Lemma 3.3 If $x > x_+$, then $\displaystyle\int_x^{x + \frac{2\pi}{\sqrt{6\lambda_0}}} S^2(\eta)(\zeta)\sin(\sqrt{6\lambda_0}\zeta)d\zeta = 0$ and

$$\int_x^{x + \frac{2\pi}{\sqrt{6\lambda_0}}} S^2(\eta)(\zeta)\cos(\sqrt{6\lambda_0}\zeta)d\zeta = 0.$$

Proof Let $\eta \in B$, $x > x_+$ and x_1 be any real number. Put $\sqrt{6\lambda_0} = \Lambda$. Then

$$\int_x^{x + \frac{2\pi}{\Lambda}} S^2(\eta)(\zeta)\sin\Lambda(x_1 - \zeta)d\zeta$$

$$= \frac{1}{\Lambda^2}\int_x^{x + \frac{2\pi}{\Lambda}} \sin\Lambda(x_1 - \zeta)\Big[\int_0^{\zeta} \sin\Lambda(\zeta - t)\Big(\frac{9}{2}\eta^2(t) + 3b(t)\Big)dt\Big]^2 d\zeta$$

$$= \frac{1}{\Lambda^2}\int_x^{x + \frac{2\pi}{\Lambda}} \sin\Lambda(x_1 - \zeta)\int_0^{\zeta} \sin\Lambda(\zeta - t)\Big(\frac{9}{2}\eta^2(t) + 3b(t)\Big)dt$$

$$\int_0^{\zeta} \sin\Lambda(\zeta - s)\Big(\frac{9}{2}\eta^2(s) + 3b(s)\Big)ds d\zeta$$

$$= \frac{1}{\Lambda^2}\int_x^{x + \frac{2\pi}{\Lambda}} \int_0^{\zeta} \int_0^{\zeta} \sin\Lambda(x_1 - \zeta)\sin\Lambda(\zeta - t)\sin\Lambda(\zeta - s)$$

$$\Big[\frac{9}{2}\eta^2(t) + 3b(t)\Big]\Big[\frac{9}{2}\eta^2(s) + 3b(s)\Big]dt ds d\zeta$$

$$= \frac{1}{4\Lambda^2} \int_x^{x+\frac{2\pi}{\Lambda}} \int_0^\zeta \int_0^\zeta [\sin\Lambda(x_1 - \zeta - s - t) + \sin\Lambda(x_1 - \zeta + s - t)$$
$$- \sin\Lambda(x_1 - 3\zeta + s + t) - \sin\Lambda(x_1 + \zeta - s - t)]$$
$$\left[\frac{9}{2}\eta^2(t) + 3b(t)\right]\left[\frac{9}{2}\eta^2(s) + 3b(s)\right]dtdsd\zeta$$

(since $4\sin\alpha\sin\beta\sin\gamma = \sin(\beta + \gamma - \alpha) + \sin(\gamma + \alpha - \beta) + \sin(\alpha + \beta - \gamma)$

$$- \sin(\alpha + \beta + \gamma)).$$

By changing order of integration, we obtain that

$$\int_x^{x+\frac{2\pi}{\Lambda}} S^2(\eta)(\zeta)\sin\Lambda(x_1 - \zeta)d\zeta = \frac{1}{4\Lambda^2}(I_1 + I_2 + I_3 + I_4 + I_5)$$

where $I_1 = \int_0^x \int_0^x \int_x^{x+\frac{2\pi}{\Lambda}} P(x_1, \zeta, s, t)d\zeta dtds,$

$$I_2 = \int_x^{x+\frac{2\pi}{\Lambda}} \int_0^x \int_s^{x+\frac{2\pi}{\Lambda}} P(x_1, \zeta, s, t)d\zeta dtds,$$

$$I_3 = \int_x^{x+\frac{2\pi}{\Lambda}} \int_0^x \int_t^{x+\frac{2\pi}{\Lambda}} P(x_1, \zeta, s, t)d\zeta dsdt,$$

$$I_4 = \int_x^{x+\frac{2\pi}{\Lambda}} \int_x^t \int_t^{x+\frac{2\pi}{\Lambda}} P(x_1, \zeta, s, t)d\zeta dsdt,$$

$$I_5 = \int_x^{x+\frac{2\pi}{\Lambda}} \int_x^s \int_s^{x+\frac{2\pi}{\Lambda}} P(x_1, \zeta, s, t)d\zeta dtds, \text{ and}$$

$$P(x_1, \zeta, s, t) = [\sin\Lambda(x_1 - \zeta - s - t) + \sin\Lambda(x_1 - \zeta + s - t)$$

$$- \sin\Lambda(x_1 - 3\zeta + s + t) - \sin\Lambda(x_1 + \zeta - s - t)]$$

$$\left[\frac{9}{2}\eta^2(t) + 3b(t)\right]\left[\frac{9}{2}\eta^2(s) + 3b(s)\right].$$

Note that,

(i) by changing of variable, it can easily be shown that $I_1 = 0$, and

(ii) by symmetry of s and t, it can easily be shown that $I_2 = I_3$ and $I_4 = I_5$.

Thus, by integrating I_2 and I_4 with respect to ζ, we have

$$\int_x^{x+\frac{2\pi}{\Lambda}} S^2(\eta)(\zeta)\sin\Lambda(x_1 - \zeta)d\zeta = \frac{1}{2\Lambda^3}\left(I_6 + \frac{81}{2}I_7\right) \text{ where}$$

$$I_6 = \int_x^{x+\frac{2\pi}{\Lambda}} \int_0^x (Q(x_1, x, s, t) + R(x_1, s, t))\left(\frac{9}{2}\eta^2(t) + 3b(t)\right)\left(\frac{9}{2}\eta^2(s) + 3b(s)\right)dsdt,$$

$$I_7 = \int_x^{x+\frac{2\pi}{\Lambda}} \int_x^s (Q(x_1, x, s, t) + R(x_1, s, t))\eta^2(t)\eta^2(s)dtds$$

(since $x > x_+$, $b(x) = 0$),

$$Q(x, x_1, s, t) = \cos \Lambda(x_1 - x - s - t) + \cos \Lambda(x_1 - x + s - t)$$
$$- \frac{1}{3} \cos \Lambda(x_1 - 3x + s + t) + \cos \Lambda(x_1 + x - s - t), \text{ and}$$
$$R(x_1, s, t) = -\frac{2}{3} \cos \Lambda(x_1 - 2s + t) - 2 \cos \Lambda(x_1 - t).$$

Since $\eta \in B$, if we change variable and integrate I_6 with respect to t first we obtain that $I_6 = 0$.

By the symmetry of the region of integration, we have

$$\frac{1}{2} \int_x^{x+\frac{2\pi}{\Lambda}} \int_x^{x+\frac{2\pi}{\Lambda}} Q(x_1, x, s, t) \eta^2(s) \eta^2(t) dt ds$$
$$= \int_x^{x+\frac{2\pi}{\Lambda}} \int_x^s Q(x_1, x, s, t) \eta^2(s) \eta^2(t) dt ds.$$

Then I_7 can be written as $I_7 = \frac{1}{2} I_8 + I_9$ where

$$I_8 = \int_x^{x+\frac{2\pi}{\Lambda}} \int_x^{x+\frac{2\pi}{\Lambda}} Q(x_1, x, s, t) \eta^2(s) \eta^2(t) dt ds, \text{ and}$$
$$I_9 = \int_x^{x+\frac{2\pi}{\Lambda}} \int_x^s R(x_1, s, t) \eta^2(s) \eta^2(t) dt ds.$$

Here, since $\eta \in B$, if we change variable we obtain that I_8 vanishes.

By the definition of space B, each $\eta \in B$ is of a Fourier approximation for which η^2 can be represented by

$$\eta^2(x) = \sum_{n=1}^{\infty} (E_n \sin 2n\Lambda x + F_n \cos 2n\Lambda x) \; ; \; x > x_+$$

equality here is in the sense of almost everywhere. Hence

$$\int_x^s \{\cos, \sin\}(\Lambda t) \eta^2(t) dt$$
$$= \int_x^s \{\cos, \sin\}(\Lambda t) \sum_{n=1}^{\infty} (E_n \sin 2n\Lambda t + F_n \cos 2n\Lambda t) dt$$
$$= F_0(x) + \sum_{n=1}^{\infty} (G_n \sin(2n-1)\Lambda s + H_n \cos(2n-1)\Lambda s).$$

Thus I_9 is, then, of the form

$$I_9 = -\frac{2}{3} \int_x^{x+\frac{2\pi}{\Lambda}} \eta^2(s) \cos \Lambda(x_1 - 2s) \int_x^s \eta^2(t) \cos \Lambda t \, dt \, ds$$
$$+ \frac{2}{3} \int_x^{x+\frac{2\pi}{\Lambda}} \eta^2(s) \sin \Lambda(x_1 - 2s) \int_x^s \eta^2(t) \sin \Lambda t \, dt \, ds$$
$$- 2 \int_x^{x+\frac{2\pi}{\Lambda}} \eta^2(s) \cos \Lambda x_1 \int_x^s \eta^2(t) \cos \Lambda t \, dt \, ds$$
$$- 2 \int_x^{x+\frac{2\pi}{\Lambda}} \eta^2(s) \sin \Lambda x_1 \int_x^s \eta^2(t) \sin \Lambda t \, dt \, ds$$

$$= 0$$

since the integrands in all the above integrals with respect to s in a period are either products of even and odd harmonics or product of constants and harmonics. The lemma is proved by letting $x_1 = 0$ and $x_1 = \dfrac{\pi}{2\Lambda}$, respectively.

$\square$

Theorem 3.1 $6\lambda_0\eta + \eta_{xx} = -\dfrac{9}{2}\eta^2 - 3b(x)$ has a solution if $\sqrt{6\lambda_0}$ is sufficiently large.

Proof $\|S(\eta_1) - S(\eta_2)\| = \sup\limits_{x\in\mathbb{R}} \left| \dfrac{9}{2\sqrt{6\lambda_0}} \displaystyle\int_0^x \sin\sqrt{6\lambda_0}(x-\xi)(\eta_1^2(\xi) - \eta_2^2(\xi))d\xi \right|$

$\leq \dfrac{9}{2\sqrt{6\lambda_0}} \sup\limits_{x\in\mathbb{R}} \left\{ \left| \displaystyle\int_0^{x_+} \sin\sqrt{6\lambda_0}(x-\xi)(\eta_1^2(\xi) - \eta_2^2(\xi))d\xi \right| \right.$

$\qquad + \left| \displaystyle\int_{x_+}^{x_+ + \frac{2\pi}{\sqrt{6\lambda_0}}} \sin\sqrt{6\lambda_0}(x-\xi)(\eta_1^2(\xi) - \eta_2^2(\xi))d\xi \right|$

$\qquad + \left. \left| \displaystyle\int_{x_+ + \frac{2\pi}{\sqrt{6\lambda_0}}}^{x_+ + \frac{2\pi n}{\sqrt{6\lambda_0}}} \sin\sqrt{6\lambda_0}(x-\xi)(\eta_1^2(\xi) - \eta_2^2(\xi))d\xi \right| \right\}$

$\qquad\qquad$ for some $n \in \mathbb{N}$

$\leq \dfrac{9N}{2\sqrt{6\lambda_0}} \|\eta_1 - \eta_2\| \left[\sup\limits_{x\in\mathbb{R}} \displaystyle\int_0^{x_+} |\sin\sqrt{6\lambda_0}(x-\xi)| d\xi \right.$

$\qquad + \left. \sup\limits_{x\in\mathbb{R}} \displaystyle\int_{x_+}^{x_+ + \frac{2\pi}{\sqrt{6\lambda_0}}} |\sin\sqrt{6\lambda_0}(x-\xi)| d\xi \right]$

$\leq \dfrac{9N}{2\sqrt{6\lambda_0}} \left(x_+ + \dfrac{2\pi}{\sqrt{6\lambda_0}} \right) \|\eta_1 - \eta_2\|.$

Hence we can see from Lemma 3.1, 3.2 and 3.3 that S is a contraction mapping if $\sqrt{6\lambda_0} \geq \left[\dfrac{9}{2}N(x_+ + \dfrac{2\pi}{\sqrt{6\lambda_0}}) + \dfrac{3\|b\|}{N}x_+ \right]$ and the integral equation $\eta = S(\eta)$ has the unique solution in B_N.

$\square$

3.2 Numerical Procedure

We use only the system of RK4 to calculate the solution in this case. Consider

$$6\lambda\eta - \eta_{xx} = \frac{9}{2}\eta^2 + 3b(x)$$

with the initial conditions $\eta(-1) = 0$ and $\eta'(-1) = 0$.

We solve the above initial value problem by discretizing the physical domain into a finite number of mesh points. To calculate the function $\eta(x)$ at each mesh point, we first let $w(x) = \eta_x$. Then $w_x(x) = \eta_{xx} = z(x, \eta)$, where $z(x, \eta) = -\frac{9}{2}\eta^2 + 6\lambda\eta - 3b(x)$. We use the formulas to calculate $w(x)$ as follow:

$$w(x + h) = w(x) + \frac{1}{6}(G_1 + 2G_2 + 2G_3 + G_4),$$

where $G_1 = hz(x, \eta)$,

$$G_2 = hz\left(x + \frac{h}{2}, \eta + \frac{1}{2}G_1\right),$$
$$G_3 = hz\left(x + \frac{h}{2}, \eta + \frac{1}{2}G_2\right) \text{ and}$$
$$G_4 = hz(x + h, \eta + G_3).$$

Next, since $w(x) = \eta_x$, to obtain the numerical solution of $\eta(x)$ we use the above formulas again by replacing all w's by η and z's by w. Numerical results will be shown and discussed in the next section.

3.3 Numerical Results and Discussions

In this section, numerical solutions in the subcritical flow regime are presented. We found that, when $\lambda < 0$, the flow is characterized by a train of nonlinear periodic waves behind the pressure distribution while the upstream free surface satisfies the radiation condition (see Figure 3.1 and 3.2). Figure 3.3 and 3.4 show the behavior of the free-surface for various values of λ when $\epsilon = 0.5, 1$ and 2. As we shall see later, there are critical values of λ at which the wave amplitude

diminishes. This is so-call *drag-free* solution. That is the flow possesses no wave resistance which may be of interest in practice.

When $\epsilon = 0$, uniform flow is always the solution in this case. Let us now define the wave amplitude A as the difference between the levels of the successive crest and trough. It can be seen that, for the same value of λ, the wave amplitude increases as ϵ gets bigger (i.e., larger magnitude of pressure distribution, see Figure 3.5). We observe from the relationships between wave amplitude A and the critical values λ_* of λ (Figure 3.5) such that the wave amplitude vanishes. Some of these critical values for $\epsilon = 0.1$ are shown in Table 3.1.

i	λ_{*i}
1	- 4.161
2	- 13.161
3	- 26.411
4	- 43.8

Table 3.1

In addition, similar behavior can be found for the steepness S of the waves, defined as the ratio of the height between a crest and a trough and the wave length. This is shown in Figure 3.6.

When $\lambda > \lambda_{*1}$, the wave amplitude A increases with λ whereas the steepness S increases to its maximum value and then decreases as $\lambda \rightarrow \lambda_{*2}$. For each ϵ, when λ lies between the two consecutive critical values $\lambda_{*i} < \lambda < \lambda_{*i-1}$ for $i = 2, 3, ...$, the amplitude and steepness increase to their peaks and decrease as λ decreases between the values λ_{*i-1} and λ_{*i}. Similarly, the results for $\epsilon < 0$ are presented in Figure 3.7-3.8. We found that the behavior of these numerical values is qualitatively similar for $\epsilon > 0$ except the reverse signs of the wave amplitude

A. Thus, it is sufficient to present results for the case $\epsilon > 0$.

Typical profiles of the drag-free solution as λ approaches λ_{*1}, λ_{*2}, λ_{*3}, and λ_{*4} are shown in Figure 3.9. Besides the decreasing amplitude of the deformed free surface, we observe that two *humps* occurs as $\lambda \to \lambda_{*2}$ while only one *hump* is detected when $\lambda \to \lambda_{*1}$. Since the lower bound of λ should be $-\dfrac{1}{\varepsilon}$, we conjecture that there are finitely many critical λ_{*i} such that drag-free solutions exist. This is of interest to architectural design of the moving vehicle on the free surface. In addition, the numerical results show that as $\lambda \to \lambda_{*n}$, there are n *humps* on the free surface of the drag-free solutions. It is found that this similar behavior of subcritical solutions exists in the case $\epsilon < 0$.
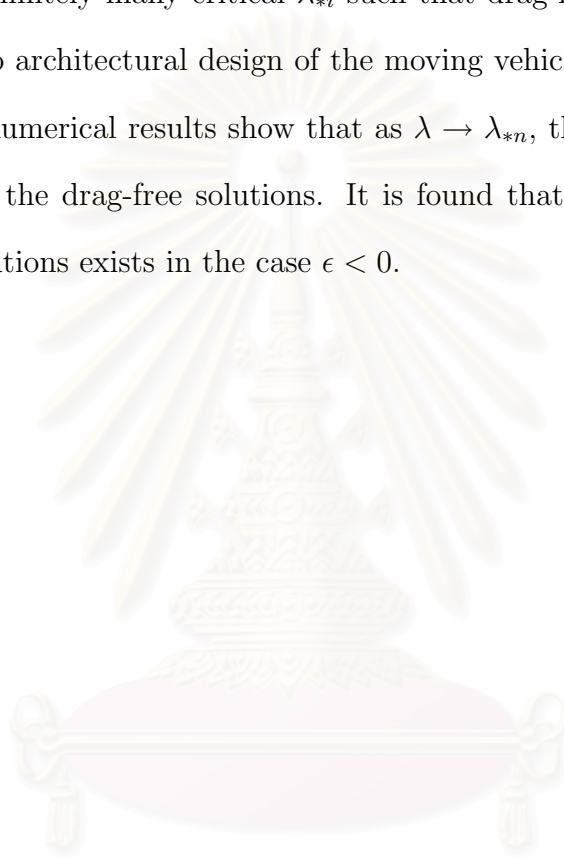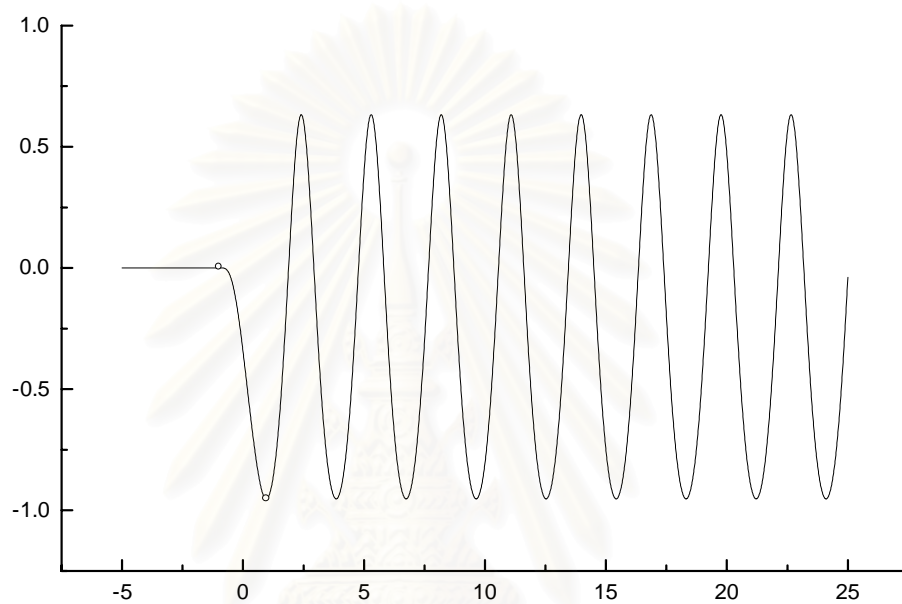
Figure 3.1: Typical free-surface profile for $\lambda = -1.1$ and $\epsilon = 2$.
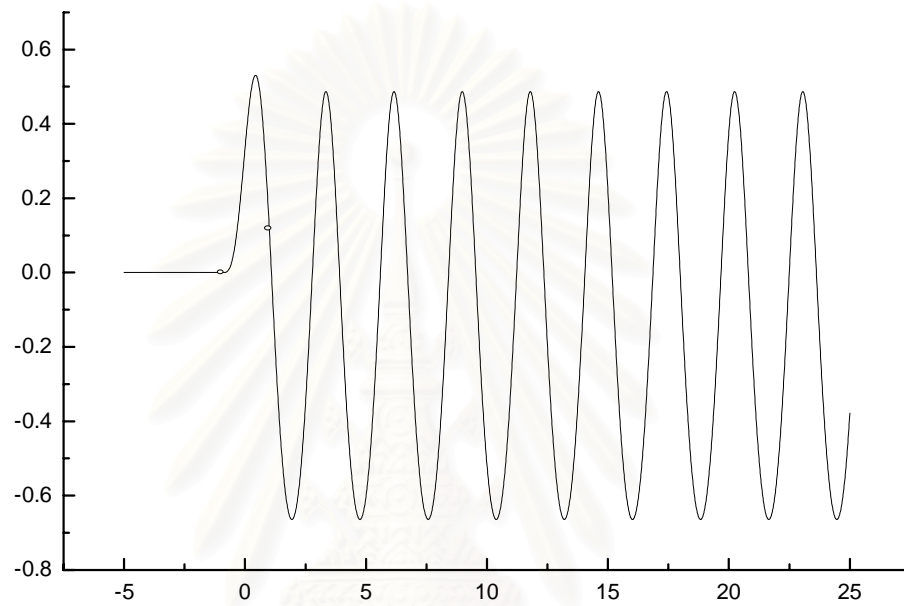
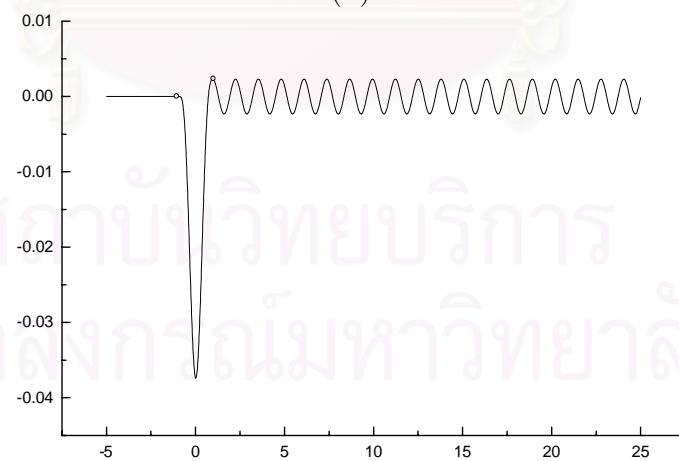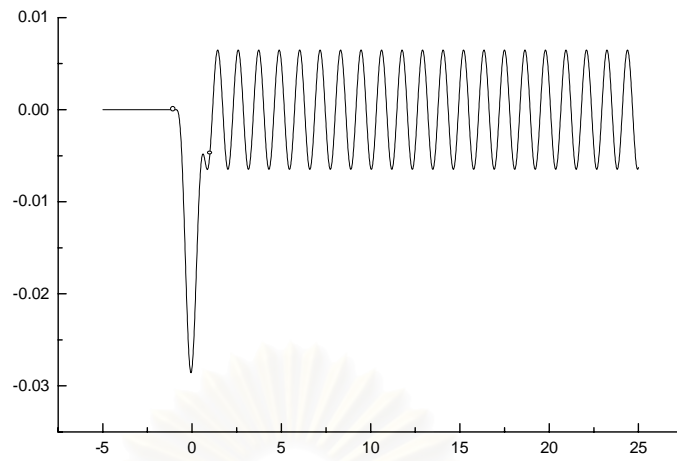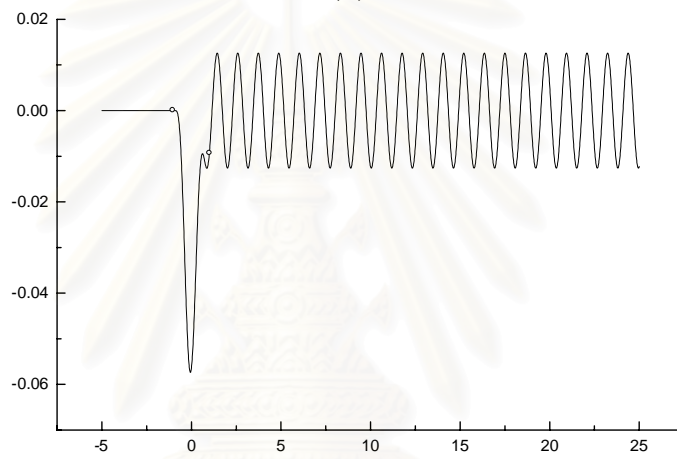Figure 3.2: Typical free-surface profile for $\lambda = -1$ and $\epsilon = -2$.
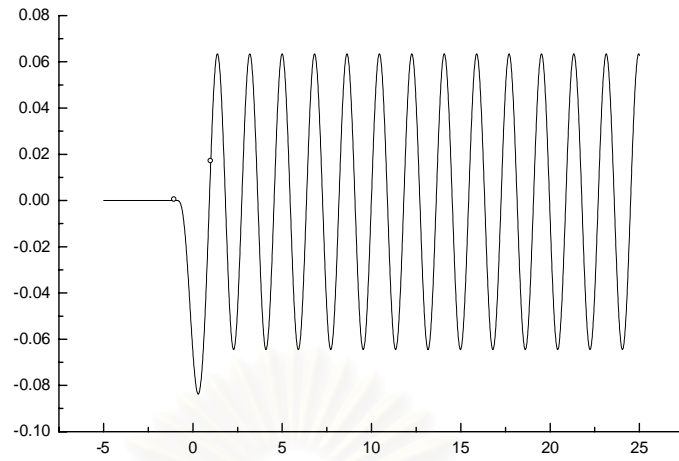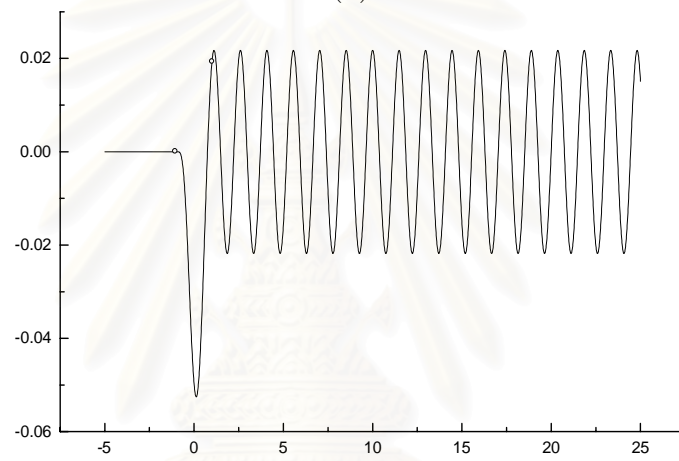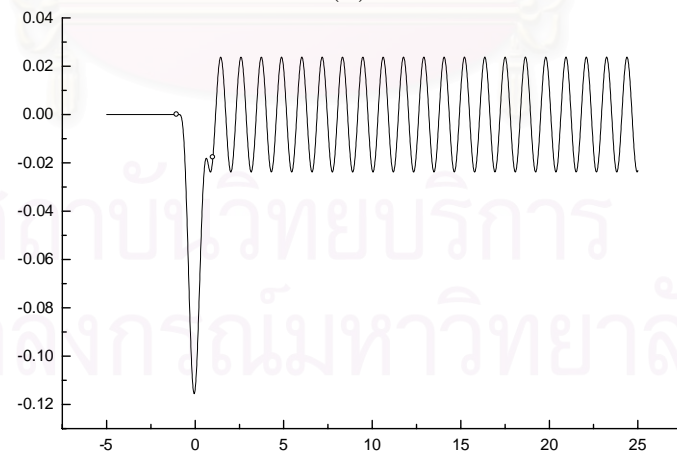
Figure 3.3: Typical free-surface profiles (a) for $\lambda = -2$, $\epsilon = 0.5$, (b) for $\lambda = -3$, $\epsilon = 0.5$, and (c) for $\lambda = -4$, $\epsilon = 0.5$.

Figure 3.4: Typical free-surface profiles (a) for $\lambda = -5$, $\epsilon = 0.5$, (b) for $\lambda = -5$, $\epsilon = 1$, and (c) for $\lambda = -5$, $\epsilon = 2$.
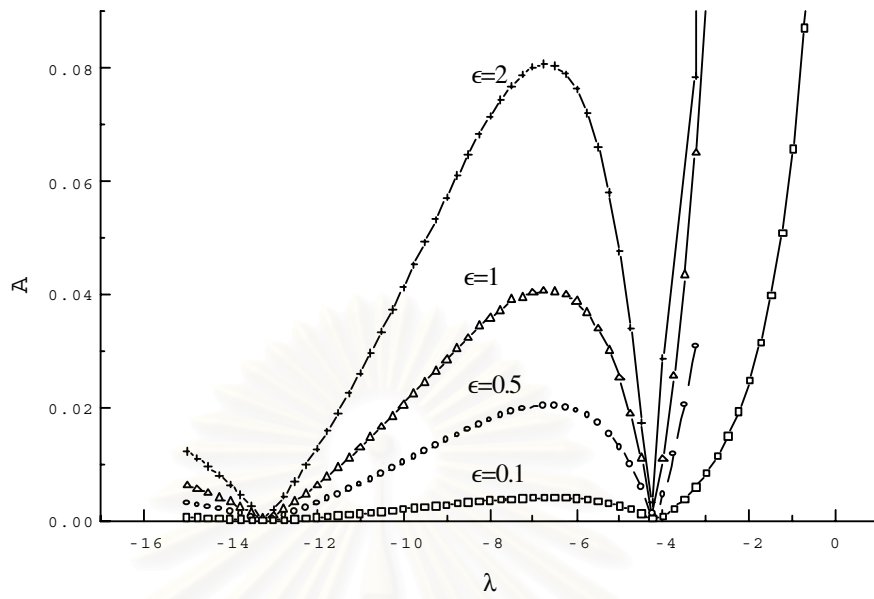
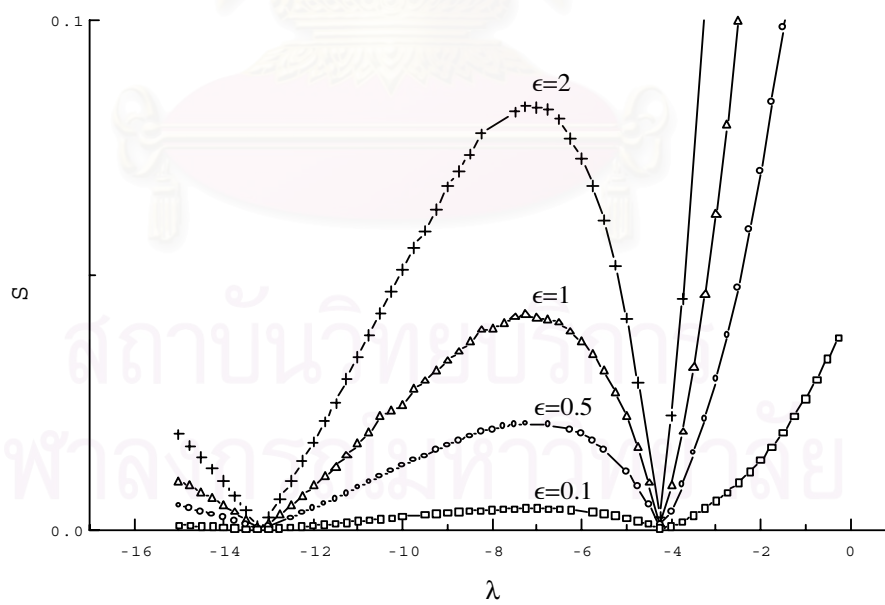Figure 3.5: Relationship between amplitude A and λ for various values of $\epsilon > 0$.

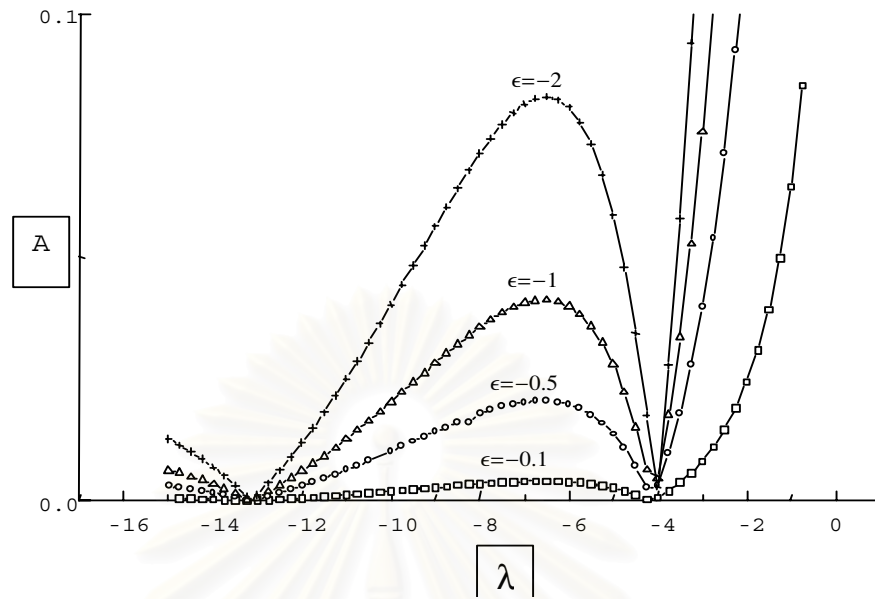Figure 3.6: Relationship between steepness S and λ for various values of $\epsilon > 0$.

Figure 3.7: Relationship between amplitude A and λ for various values of $\epsilon < 0$.

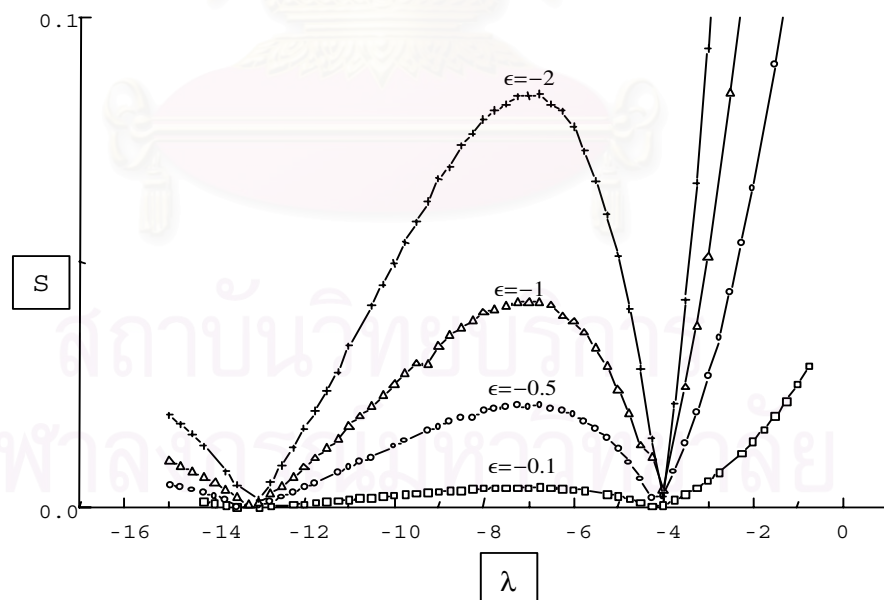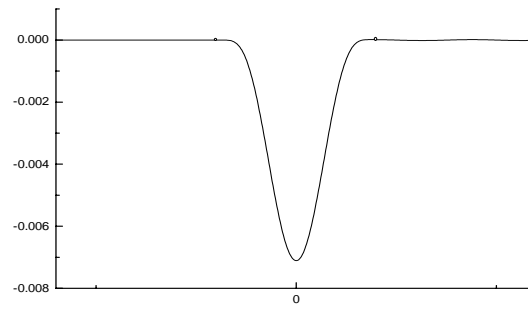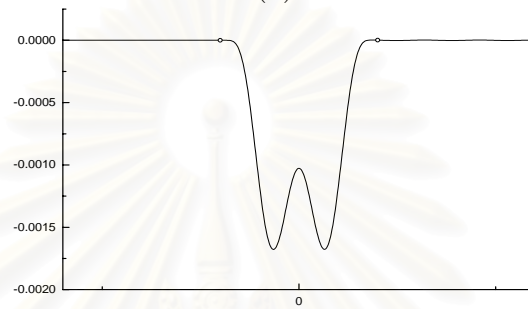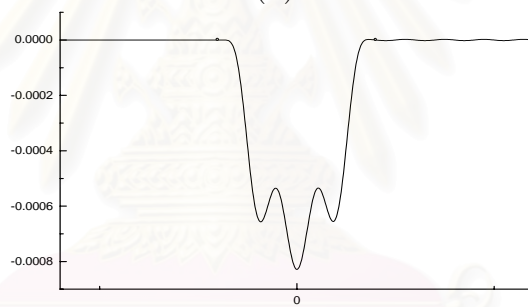Figure 3.8: Relationship between steepness S and λ for various values of $\epsilon < 0$.
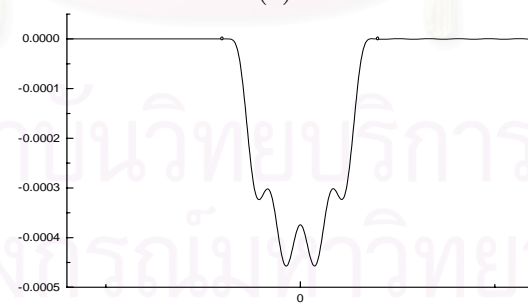
(a)

(b)

(c)

(d)

Figure 3.9: Typical free surface profiles (a) for $\lambda = \lambda_{*1}$, $\epsilon = 0.1$, (b) for $\lambda = \lambda_{*2}$, $\epsilon = 0.1$, (d) for $\lambda = \lambda_{*3}$, $\epsilon = 0.1$, and (d) for $\lambda = \lambda_{*4}$, $\epsilon = 0.1$.

CHAPTER IV

Conclusions

In this work, we assume that all non-dimensional variables and parameter possess the asymptotic expansion of the form

$$\phi = \phi_0 + \varepsilon\phi_1 + \varepsilon^2\phi_2 + ...$$

Taylor approximation with respect to variable y is used in the kinematic boundary condition. Keeping terms up to ε^2, we obtain the force stationary Korteweg-de Vries equation.

$$3\eta\eta_x - 2\lambda\eta_x + \frac{1}{3}\eta_{xxx} + b_x(x) = 0,$$

where $b(x) = \begin{cases} 0 & \text{for} \ \ |x| \geq 1 \\ \epsilon\exp\left(\dfrac{1}{x^2-1}\right) & \text{for} \ \ |x| < 1 \end{cases}$ and ϵ is a constant.

Finally, existence theorems of the solution are proved by using the fixed point theorem for a contraction mapping. To confirm these results, we calculate the solutions using the aforementioned numerical procedures. To summarize the results, we split the solution into two cases depending on their behaviors.

(i) Supercritical flow ($\lambda > 0$).

There are two different types of symmetric solutions. Solutions of the first type are characterized by $W < 0$. In addition, amplitude W increases as ϵ increases. Solutions of the second type are characterized by $W > 0$. Our numerical results show that there are nonuniqueness of solutions corresponding to same value of λ.

We conjecture that one solution is the perturbation of uniform stream while the other solution is a perturbation of solitary wave solution.

(ii) Subcritical flow ($\lambda < 0$).

Solutions in this case possess a train of nonlinear waves behind the pressure distribution. The amplitude A of the wave decreases as λ decreases. The wave amplitude ultimately become zero when the critical value λ_{*1} of λ is reached. For $\lambda < \lambda_{*1}$, the wave amplitude increases to other local maximum value and then decreases monotonically to zero again at $\lambda = \lambda_{*2}$. In addition, the free surface, upon which the pressure distribution was applied, is deformed into two *humps*. This cycle of behavior occurres repeatedly as λ reaches another critical value with *n humps* on the free surface as $\lambda \to \lambda_{*n}$. Similar behavior can be found for the steepness S of the waves.

Finally, it should be noted here that our results are obtained by using small amplitude theory. One can further investigate in the higher order of ε, which, of course, will involve more calculations. However, our small amplitude results seems to have qualitatively similar behavior as those of finite amplitude (Von Kerczek and salvesen (1977), Schwartz (1981), Asavanant and Vanden-Broeck (1994), and Asavanat, et, al. (2001)). For further study, one can include the surface tension effect into the problem. This may probably require the fifth order KdV to incorporate with the extra parameter in the problem.

REFERENCES

C. Von Kerczek and Nils Salvesen. Nonlinear free-surface effects-the dependence
on Froude number. Proc. 2$^{\underline{nd}}$ Int. Conf. On Numerical Ship Hydrodyna-
mics Berkeley, 1977 : 292-300.

H. Lamb. Hydrodynamics. New York : Dover Publications, 1945.

J. Asavanant and J.M. Vanden-Broeck. Free-surface flows past a surface-piercing
object of finite length. Journal of Fluid Mechanics 273, 1994 : 109-124.

J. Asavanant, M. Maleewong and J. Choi Computation of free-surface flows due
to pressure distribution. Comm. Korean Math. Soc. 16 No. 1, 2001 :
137-152.

L.K. Forbes and L.W. Schwartz. Free-surface flow over a semicircular obstruction.
Journal of Fluid Mechanics 14, 1982 : 299-314.

L.W. Schwartz. Nonlinear solution for an applied overpressure on moving stream.
Journal of Engineering Mathemtics 12, 1981 : 147-156.

VITA

Name   : Mr. Ratinan Boonklurb

Degree obtained : Bachelor of Science (2$^{\underline{nd}}$ Class Degree Honours), 1998,

  Chulalongkorn University, Bangkok, Thailand.

Scholarship   : University Development Commission (U.D.C.)

  Thai government, 1999-2000.